Optimal Time Selection for ISAR Imaging of Ship Target via Novel Approach of Centerline Extraction With RANSAC Algorithm

Rui Cao, *Graduate Student Member, IEEE*, Yong Wang, *Senior Member, IEEE*, Yun Zhang, *Member, IEEE*, and Mao Jian

***Abstract*—Optimal time selection for inverse synthetic aperture radar imaging of ship target is significant for the determination of image project plane, and the performance of it is dependent on the accuracy of ship centerline extraction. In this article, a novel optimal time selection method based on the random sample consensus (RANSAC) technique is proposed, which can extract the ship centerline with high accuracy in the case of ship superstructure and low signal to noise ratio. First, a necessary distance threshold is determined for the RANSAC algorithm combined with the ship body width estimation. Then, a novel cost function is proposed according to the amplitude characteristic of radar image, which can alleviate the influence of randomness. Finally, the robustness of the optimal time selection method is demonstrated by the results of simulated and real measured data.**

***Index Terms*—Low signal to noise ratio (SNR), optimal time selection, radar image, random sample consensus (RANSAC) algorithm, ship centerline extraction, ship superstructure.**

NOMENCLATURE

ISAR	Inverse synthetic aperture radar.
SNR	Signal to noise ratio.
LS	Least squares.
RANSAC	Random sample consensus.
Δf_d	Doppler spread.
t_m	Slow time.
$C_{\rm s}$	Constant related to the size of ship target.
$\omega_{\rm E}$	Effective angular motion.
$\omega_{\rm H}$	Horizontal component of $\omega_{\rm E}$.
$\omega_{\rm V}$	Vertical component of $\omega_{\rm E}$.
k	Slope of ship centerline.
ΔR_s	Number of range bins that is occupied by ship target in the ISAR image.
$C_{\rm r}$	Constant related to the aspect angle.
$l_{\rm OTSU}$	Amplitude threshold via OTSU method.
$I(m,n)$	Radar image.
m	Azimuth order, $m = 1, 2, \cdots, N_a$.
n	Range order, $n = 1, 2, \cdots, N_r$.
N_a	Number of azimuth bins.
N_r	Number of range bins.
$\mathbf{x}_t$	Position of sample, $\mathbf{x}_t = [x_t, y_t]^T$.
I_t	Amplitude of sample, $I_t = I(\mathbf{x}_t)$.
t	Sample order, $t = 1, 2, \cdots, T$.
T	Number of samples.
$D_{\max}$	Distance threshold.
$I_{\rm num}$	Iteration number in RANSAC algorithm.
i	Iteration order of RANSAC algorithm.
b	Intercept of ship centerline.
$N_{\rm in}$	Number of inliers.
$\chi_{\rm in}$	Data set of inliers.
d_t	Distance between samples and line.
$\chi_{\rm out}$	Data set of outliers.
$\boldsymbol{K}$	Matrix of slope.
$\boldsymbol{B}$	Matrix of intercept.
$D_{\rm s}$	Width of ship body.
$\boldsymbol{S}_I$	Matrix of amplitude sum.
s_I	Sum of image amplitude.
L	Iteration number of RANSAC method.
l	Iteration order of proposed approach, $l = 1, 2, \cdots, L$.
d_w	Sequence of distance threshold.
W	Number of distance threshold.
$\tilde{\boldsymbol{S}}_I$	Matrix after sorting $\boldsymbol{S}_I$.
$\{\tilde{\boldsymbol{S}}_I(w,\tilde{l})\}$	Sequence of amplitude sum.
$\tilde{l}$	$\tilde{l} = 1, 2, \cdots, L_0$.
L_0	Selected number of amplitude sum.
v_w	Variance of $\{\tilde{\boldsymbol{S}}_I(w,\tilde{l})\}_{1\times L_0}$.

Manuscript received 8 August 2022; revised 20 October 2022; accepted 4 November 2022. Date of publication 8 November 2022; date of current version 30 November 2022. This work was supported in part by the National Natural Science Foundation of China under Grant 61871146 and in part by the Fundamental Research Funds for the Central Universities under Grant FRFCU5710093720. *(Corresponding author: Yong Wang.)*

Rui Cao, Yong Wang, and Yun Zhang are with the Research Institute of Electronic Engineering Technology, Harbin Institute of Technology, Harbin 150001, China (e-mail: caor@hit.edu.cn; wangyong6012@hit.edu.cn; zhangyunhit@hit.edu.cn).

Mao Jian is with the Laboratory of Pinghu, Beijing Institute of Infinite Electric Measurement, Pinghu 314200, China (e-mail: 71898568@qq.com).

Digital Object Identifier 10.1109/JSTARS.2022.3220496

I. INTRODUCTION

RADAR imaging of the ship target is the important means for the maritime monitoring and ship management, and is applied widely in the military and civilian domain [1], [2], [3], [4], [5], [6]. Abundant radar imaging algorithms have been proposed to attain the high-quality radar image of ship target [7], [8], [9], [10], [11], [12], while these algorithms only concern about the short observation time. Actually, the issues of azimuth

defocus and low imaging efficiency will appear when the observation time is long [13], [14], [15], [16], [17]. To address this issue, the optimal time selection technique in inverse synthetic aperture radar (ISAR) is aroused [4], [18], [19], [20], [21], [22].

In particular, the optimal time selection method proposed by Pastina et al. [22] becomes a research hotspot recently as it can estimate the angular motion to achieve the ISAR image with the characteristic of ship's single view, i.e., side view or top view. The ISAR image with this feature is favorable for the target feature extraction and recognition. Pastina et al. [22] proposed the theory of angular motion estimation to export the optimal time interval that features as single view. The effective angular movement of ship can decompose into the vertical and horizontal component. In a state of prominent vertical component, the top-view ISAR image can be yielded. Conversely, in the state of prominent horizontal component, the side-view ISAR image can be achieved. Meanwhile, the theory of angular motion estimation indicates that the horizontal component can be reflected by the Doppler spread, and the vertical component is concerned with the centerline slope. For the purpose of obtaining the radar image with single view, the angular movement should be estimated accurately, which is the key procedure for the optimal time selection technique.

The ship centerline is the line between the bow and stern along the direction of ship body, which can be extracted by fitting or detecting lines [19]. Nevertheless, it is difficult to extract accurately from the ISAR image with the influence of ship superstructure and low signal to noise ratio (SNR). Here, the ship superstructure refers to the structure above the ship main body, which has the different shapes and directions compared with the ship main body and is disadvantageous for the ship centerline extraction. The low SNR is another negative factor because the noisy samples will decrease the extraction precision.

Recently, many effective methods are proposed for the ship centerline extraction, such as the least squares (LS) method [22], [23], Hough transform [24], random sample consensus (RANSAC) algorithm [25], *etc*. The LS method is the classical fitting method, which uses all the observation data to fit the straight line with the criterion of minimum variance [22]. Whereas, its performance is limited by the ship superstructure and low SNR since these circumstances will produce the abnormal data.

Then, the Hough transform is proposed, which has the steady performance under the low SNR [26]. The parameters of line are detected via searching the maximum values in the parametric domain. However, the Hough transform usually detects several different lines, which is difficult to determine the ship centerline. Moreover, the performance of Hough transform is degraded by the ship superstructure as the corresponding parameter of maximum value is influenced. Although a novel ship centerline extraction method with the Hough transform is presented in [27], which is robust for the ship superstructure, the issue of multiple optimal solutions cannot be solved.

Afterward, an iterative method named RANSAC algorithm is proposed, which can eliminate the outliers induced by the low SNR [25]. Initially, the parameters of line model are calculated via selecting samples randomly. Then, the optimal solution

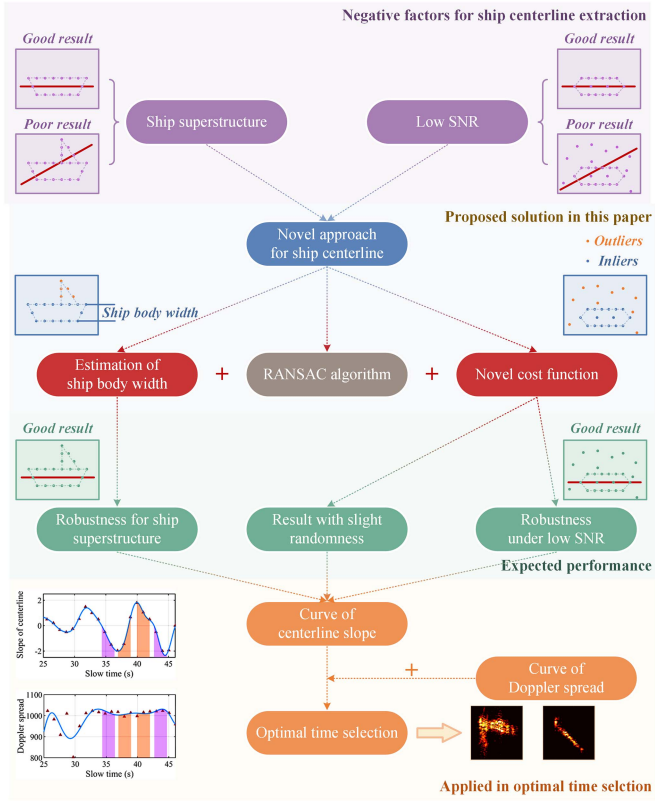

Fig. 1. Contribution of the proposed approach.

is obtained with the cost function. Here, the cost function of the conventional RANSAC algorithm is the number of inliers. Whereas, the following issues exist as well. First, a necessary distance threshold needs to be determined appropriately; otherwise, the performance of the RANSAC algorithm will be degraded obviously. Second, the fitting result is random because the samples are selected randomly to calculate the model parameters. Third, the cost function is unsuitable for the case of ship superstructure and low SNR.

In this article, a novel ship centerline extraction approach with the RANSAC algorithm is proposed, then it is successfully used in the optimal time selection for the ISAR imaging of ship target. The proposed approach utilizes the advantage adequately that the RANSAC algorithm can eliminate the outliers, which can improve the extraction precision. The main procedures of the proposed approach are as follows. First, the proposed approach can determine an optimal distance threshold for the RANSAC algorithm via the method of estimating the ship body width in [27], which can improve the extraction precision obviously. Second, a novel cost function is proposed to reduce the randomness of extraction result. Given earlier, the proposed approach can present the good performance for the ship centerline extraction, and features as good robustness under the case of ship superstructure and low SNR. The contribution of the proposed approach is summarized in Fig. 1.

The residual sections are organized as follows. First, the theory of optimal time selection technique based on the angular motion estimation is introduced in Section II. Then, the procedure of conventional RANSAC algorithm is illustrated in Section III,

and the performance of it is discussed consequently. Afterward, a novel ship extraction approach is proposed in Section IV, which overcomes the defects of the conventional RANSAC algorithm. Some results of the proposed approach and its applications in the field of optimal time selection are demonstrated via the simulated and real measured data in Sections V and VI, respectively. Finally, we draw the conclusion of this article in Section VII.

II. Theory of Optimal Time Selection Technique With Angular Motion Estimation

The effective angular motion of ship target induces the change of ISAR imaging projection plane, and produces the hybrid-view ISAR image. Usually, the ISAR image characterizing as single view is expected and conducive for target feature extraction and recognition. For this purpose, an optimal time selection technique with the angular motion estimation is proposed in [22].

The effective angular motion can be decomposed into horizontal component and vertical component, which are denoted as ω_{H} and ω_{V}, respectively. The effective angular movement is related to the Doppler spread of ship target [19], which can be expressed as follows:

$$\Delta f_d\left(t_m\right) = C_{\mathrm{s}}\omega_{\mathrm{E}}\left(t_m\right) \tag{1}$$

where Δf_d represents the Doppler spread, t_m is the slow time, C_{s} is a constant related to the size of ship target, and ω_{E} denotes the effective angular motion.

The vertical angular movement is correlated with the centerline slope, which can be represented as follows:

$$k\left(t_m\right) = \frac{\Delta f_d}{\Delta R_s} = C_{\mathrm{r}}\omega_{\mathrm{V}}\left(t_m\right) \tag{2}$$

where k expresses the slope of ship centerline, ΔR_s represents the number of range bins that are occupied by ship target in the ISAR images, and C_{r} is a constant related to the aspect angle.

Therefore, the effective angular movement can be measured with the Doppler spread, the vertical component can be observed via the centerline slope, and the horizontal component can be obtained from the relative relationship between them.

The time interval that can generate the single-view ISAR image is denoted as the optimal time selection, which can be chosen via the state of angular motion. Specifically, the top-view ISAR image can be achieved by the preponderant vertical component, corresponding to the maximum centerline slope and smaller Doppler spread. The side-view ISAR image can be acquired by the preponderant horizontal component, corresponding to the zero-crossing centerline slope and larger Doppler spread.

As illustrated earlier, the achievement of optimal time interval depends on the estimation of angular motion. Hence, the ship centerline extraction is the key procedure for achieving the single-view ISAR image, which can be implemented via the straight-line fitting. Whereas, some interference factors cause the challenge of extraction precision, such as ship superstructure and low SNR environment. To solve this problem, a novel approach of centerline extraction with RANSAC algorithm is addressed in this article, which will be elaborated in Sections III and IV.

III. Conventional RANSAC Algorithm and Performance Analysis

The proposed approach involves the conventional RANSAC algorithm, which is a straight-line fitting method as well. In this section, the radar image preprocessing is introduced first, then the theory and procedure of conventional RANSAC algorithm are described, and the performance is discussed finally.

A. Radar Image Preprocessing

First, the amplitude threshold is selected, and the samples of ship target are extracted. Here, the amplitude threshold can be determined with the OTSU method in [28]. The OTSU method is a kind of unsupervised and nonparametric method, which is simple, stable, automatic, and widely used in the field of image processing. It selects the criterion of between-class variance to analyze the "goodness" of amplitude threshold, and the optimal threshold is determined automatically via maximizing the between-class variance. Here, the amplitude threshold is denoted as l_{OTSU}, and the radar image is represented as $I(m,n)$, where $n = 1, 2, \cdots, N_r$, $m = 1, 2, \cdots, N_a$, N_r and N_a are the numbers of range and azimuth bins, respectively. With the condition of $I(m,n) \geq l_{\mathrm{OTSU}}$, the amplitude sequence and position sequence can be generated as $\{I_1, I_2, \cdots, I_T\}$ and $\{\boldsymbol{x}_1, \boldsymbol{x}_2, \cdots, \boldsymbol{x}_T\}$, respectively. Here, the position of sample is expressed as $\boldsymbol{x}_t = [x_t, y_t]^T$, the amplitude of sample is $I_t = I(\boldsymbol{x}_t) = I(x_t, y_t)$, where $t = 1, 2, \cdots, T$.

Afterward, the sequences of amplitude and position can be utilized for extracting the ship centerline. Since the RANSAC algorithm has the ability of eliminating the outliers, it is appropriate for extracting the ship centerline. Whereas, the performance of conventional RANSAC algorithm is degraded in the case of ship superstructure and low SNR. For restraining these impacts, a novel ship centerline extraction approach is proposed with the estimation of ship body width and the criterion of image amplitude, which will be elaborated in Section IV.

B. Conventional RANSAC Algorithm and Performance Analysis

The RANSAC algorithm was proposed first by Fischler and Bolles, which is an iteration method. In the RANSAC algorithm, the samples can be classified as the normal samples and abnormal samples, and named as inliers and outliers, respectively [25]. First, several samples are selected to calculate the model parameters. Then, the samples satisfied with certain condition are reserved as inliers, and other samples are eliminated as outliers. When the precision is achieved, the optimal model parameters can be obtained.

Considering the ship centerline is a straight line, the model is satisfied as follows:

$$y = kx + b \tag{3}$$

where b and k are the intercept and slope, respectively.

The flowchart of the conventional RANSAC algorithm is displayed in Fig. 2, and the main steps are as follows.

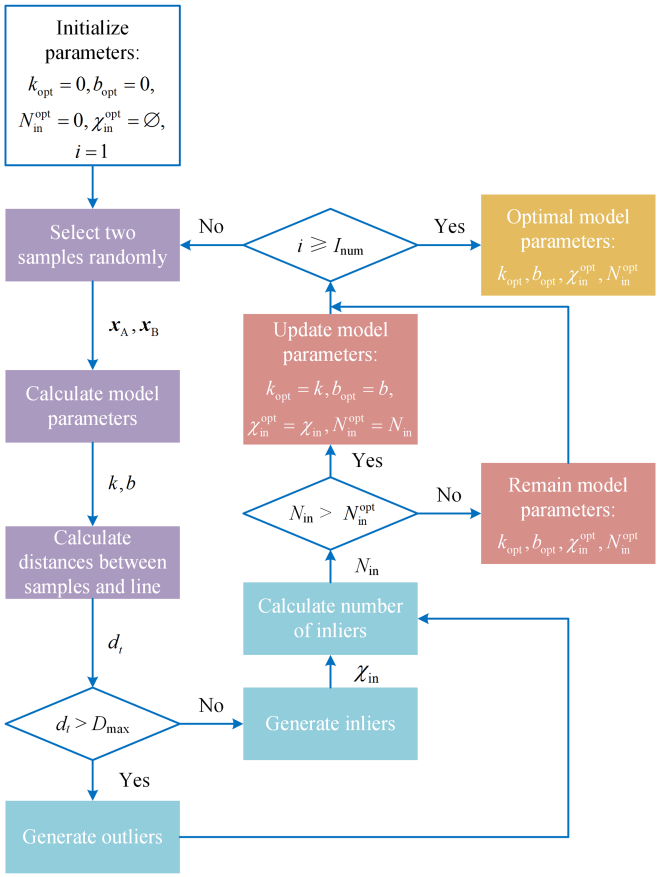

Fig. 2. Flowchart of conventional RANSAC algorithm.

Step 1: Initialize the parameters.

The distance threshold and iteration number are set as $D_{\max}$ and I_{num}, respectively. The following parameters are initialized as $i=1$, $k_{\text{opt}}=0$, $b_{\text{opt}}=0$, $N_{\text{in}}^{\text{opt}}=0$, $\chi_{\text{in}}^{\text{opt}}=\emptyset$. Here, i is the iteration order, k_{opt} and b_{opt} are the optimal slope and intercept of the fitting line, $N_{\text{in}}^{\text{opt}}$ and $\chi_{\text{in}}^{\text{opt}}$ represent the number and data set of inliers, respectively.

Step 2: Select two samples randomly, and calculate the model parameters.

The selected samples are denoted as $\boldsymbol{x}_{\text{A}}$ and $\boldsymbol{x}_{\text{B}}$, respectively and the parameters of line are calculated as follows:

$$k=\frac{y_{\text{A}}-y_{\text{B}}}{x_{\text{A}}-x_{\text{B}}} \tag{4}$$

$$b=y_{\text{A}}-kx_{\text{A}}. \tag{5}$$

Step 3: Calculate the distances between the samples and line.

The distance is computed as follows:

$$d_t=\frac{|kx_t-y_t+b|}{\sqrt{1+k^2}}. \tag{6}$$

Step 4: Compare d_t with $D_{\max}$, and generate the inliers and outliers.

If $d_t \leq D_{\max}$, the sample of $\boldsymbol{x}_t$ will be decided as the inlier and involved in the inlier set of χ_{in}. Then, the inlier set of χ_{in} is generated.

Otherwise, the data of $\boldsymbol{x}_t$ will be regarded as the outlier and added into the outlier set of χ_{out}. Then, the outlier set of χ_{out} is formed.

Step 5: Calculate the number of inliers as N_{in}, and compare N_{in} with $N_{\text{in}}^{\text{opt}}$.

If $N_{\text{in}} > N_{\text{in}}^{\text{opt}}$, the model parameters are updated as $k_{\text{opt}}=k$, $b_{\text{opt}}=b$, $\chi_{\text{in}}^{\text{opt}}=\chi_{\text{in}}$ and $N_{\text{in}}^{\text{opt}}=N_{\text{in}}$.

Otherwise, the values of k_{opt}, b_{opt}, $\chi_{\text{in}}^{\text{opt}}$ and $N_{\text{in}}^{\text{opt}}$ are unchanged.

Obviously, the number of inliers is regarded as the cost function of the conventional RANSAC algorithm.

Step 6: Compare i with I_{num}.

If $i < I_{\text{num}}$, the steps are repeated from *Step 2* and *Step 6*.

Otherwise, the RANSAC algorithm is finished, and the optimal parameters of k_{opt}, b_{opt}, $\chi_{\text{in}}^{\text{opt}}$, and $N_{\text{in}}^{\text{opt}}$ are exported.

C. Performance Analysis of Conventional RANSAC Algorithm

However, the following issues need to be solved in the conventional RANSAC algorithm.

a) The distance threshold in *Step 1* needs to be determined appropriately, otherwise the fitting performance will be poor.

b) The fitting result is random due to the operation of random selection in *Step 2*.

c) The cost function in *Step 5* is the number of inliers, which is unsuitable for extracting the ship centerline. The reason is that the ship superstructure and noisy samples may be regarded as the inliers and increase the number of inliers consequently, which degrades the performance.

Here, an experiment is designed to illustrate the aforementioned issues. The samples are consistent with the line model of $y=2x+3$, and the environmental noise exists as the outliers. The different distance thresholds are selected, and the fitting results are given in Fig. 3. Here, the green dot is the sample, the red line represents the line model of $y=2x+3$, the blue dotted line is the fitting result via the conventional RANSAC algorithm, and the blue shadow shows the confidence area of the fitting line model that is determined by the distance threshold. The samples are fitted accurately in Fig. 3(a) owing to the appropriate threshold of $D_{\max}=1$, whereas the samples are fitted incorrectly in Fig. 3(b) due to the inappropriate threshold of $D_{\max}=50$. Obviously, the fitting result is related to the distance threshold, which should be selected appropriately. Moreover, the fitting results in Fig. 3(b) and (c) are different despite the same distance threshold of $D_{\max}=50$, which is induced by the random selection of data in *Step 2* and the inappropriate cost function in *Step 5*.

The estimated slopes of the conventional RANSAC algorithm with different distance thresholds are listed in Table I, and the real value of slope is 2.0000. According to the absolute and relative error, the inappropriate threshold will degrade the estimated precision, and the randomness will influence the estimated accuracy as well.

Therefore, the conventional RANSAC algorithm is ineffective for extracting the ship centreline predictably.

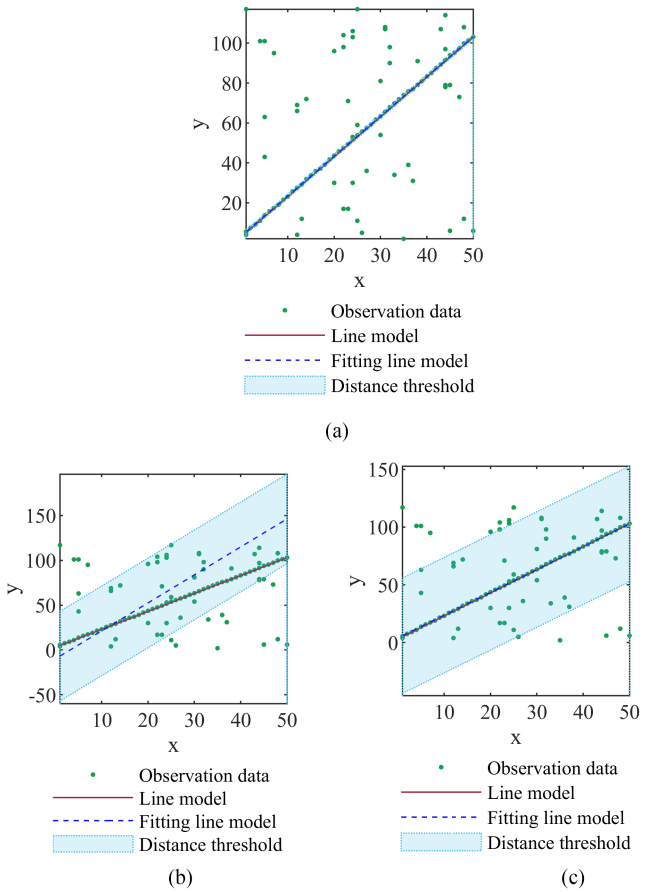

Fig. 3. Fitting results of conventional RANSAC algorithm with different distance thresholds. (a) Fitting result with appropriate distance threshold. (b) Fitting result 1 with inappropriate distance threshold. (c) Fitting result 2 with inappropriate distance threshold. (Corresponding to Table I).

TABLE I
ESTIMATION RESULTS OF CONVENTIONAL RANSAC ALGORITHM WITH DIFFERENT DISTANCE THRESHOLDS

Category	$D_{\max}=1$	$D_{\max}=50$	
		First fitting result	Second fitting result
Estimated slope	1.9927	3.1233	1.9756
Absolute error	0.0073	1.1233	0.0244
Relative error (%)	0.3652	56.1643	1.2189

IV. NOVEL APPROACH OF CENTERLINE EXTRACTION WITH RANSAC ALGORITHM

In this section, a novel ship centerline extraction approach with the RANSAC algorithm is addressed for extracting the ship centerline more preciously. First, the estimation method of ship body width in [27] is applied to determine the optimal distance threshold. Second, a novel cost function is proposed based on the characteristic of image amplitude. On this basis, the influence of randomness, ship superstructure, and low SNR can be suppressed, and the extraction precision of ship centerline can be improved consequently.

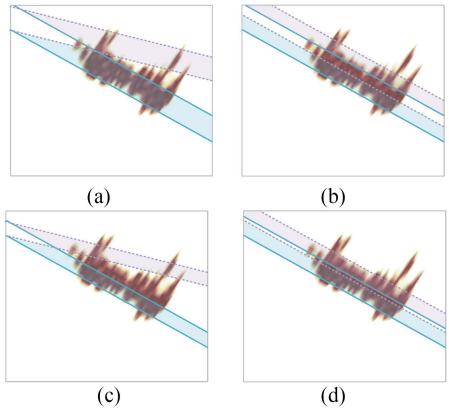

Fig. 4. Changes of amplitude sum under different cases. (a) Case 1: Changing the slope when the optimal width is obtained. (b) Case 2: Changing the intercept when the optimal width is obtained. (c) Case 3: Changing the slope when the suboptimal width is obtained. (d) Case 4: Changing the intercept when the suboptimal width is obtained.

A. Principle of Estimating Ship Body Width

Based on the method in [27], the width of ship body is related to the amplitude sum of samples that are covered by the line group. The sum of image amplitude is expressed as follows:

$$s_I(k, b_1; D_s) = \sum_{x_t} \sum_{y_t \in [kx_t+b_1, kx_t+b_s]} I(x_t, y_t) \quad (7)$$

where $b_s = b_1 + D_s$, $b_1 \le b_s$, and D_s is the width of ship body. Here, the line group consists of the lines whose slope is k and intercepts are $[b_1, b_s]$.

The amplitude sum changes with the slope and intercept, and the analyzing results under different cases are given in Fig. 4. The coverage area of line group with the optimal slope and intercept is shown as the blue lines, and the coverage area of line group with the suboptimal slope and intercept is shown as the purple dotted lines. The different areas of the two coverage areas are represented as the blue and purple shadow area, respectively.

The assumption is that the number of samples in the ship superstructure is apparently less than the number of samples in the ship body, which conforms to the most ship targets in the actual scenario.

When the width of ship body is optimal, the changes induced by the slope and intercept are demonstrated in Fig. 4(a) and (b), respectively. Apparently, the blue shadow area covers the main ship body, whereas the purple shadow area covers the part of ship superstructure. Since the area and sample number of ship body are larger than those of ship super structure, the difference of the two shadow areas is obvious. When the width of ship body is suboptimal, the changes induced by the slope and intercept are given in Fig. 4(c) and (d), respectively. Relatively, the difference of the two shadow areas is smaller compared with the case of optimal ship body width.

Hence, the amplitude sum is influenced severely with the change of slope and intercept, which is the principle of estimating the ship body width proposed in [27].

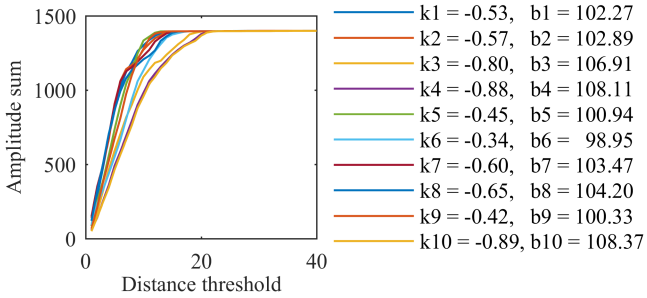

Fig. 5. Relationship between amplitude sum and distance threshold.

B. Proposed Approach

First, the optimal distance threshold of D_{opt} is obtained via estimating the ship body width with the principle in [27]. For the RANSAC algorithm, the calculation of amplitude sum in (7) is rewritten as follows:

$$s_I\left(k, b; D_{\max}\right) = \sum_{(x_t, y_t)\in\chi_{\text{in}}} I\left(x_t, y_t\right). \tag{8}$$

According to the principle in [27], the slopes and intercepts should be changed, which can be achieved with repeating the RANSAC algorithm to produce random results. For each distance threshold, the RANSAC algorithm is implemented repeatedly. Then, the matrix of amplitude sum can be generated as follows:

$$\boldsymbol{S}_I = \begin{bmatrix} s_I\left(k_{11}, b_{11}; d_1\right) & \cdots & s_I\left(k_{1L}, b_{1L}; d_1\right) \\ \vdots & \ddots & \vdots \\ s_I\left(k_{W1}, b_{W1}; d_W\right) & \cdots & s_I\left(k_{WL}, b_{WL}; d_W\right) \end{bmatrix}. \tag{9}$$

The distance threshold is set as $d_w (w = 1, 2, \cdots, W)$, and W is the number of distance threshold. The RANSAC algorithm is repeated for L times, and $l = 1, 2, \cdots, L$. Correspondingly, the matrices of slope and intercept can be obtained as follows:

$$\boldsymbol{K} = \begin{bmatrix} k_{11} & \cdots & k_{1L} \\ \vdots & \ddots & \vdots \\ k_{W1} & \cdots & k_{WL} \end{bmatrix} \tag{10}$$

$$\boldsymbol{B} = \begin{bmatrix} b_{11} & \cdots & b_{1L} \\ \vdots & \ddots & \vdots \\ b_{W1} & \cdots & b_{WL} \end{bmatrix}. \tag{11}$$

Based on (8), the value of $s_I(k_{wl}, b_{wl}; d_w)$ is increased with the larger width of d_w, and stable at the maximum value of $s_{\max} = \sum_{x_t}\sum_{y_t} I(x_t, y_t)$. This relationship is sketched in Fig. 5, which shows the amplitude sum curves with different groups of slope and intercept. Apparently, the curve gradually rises, tends to be stable, and finally reaches the maximum value. For the ship with superstructure, the amplitude sum of $s_I(k_{wl}, b_{wl}; D_{\text{opt}})$ is smaller than $s_{\max}$, where D_{opt} is the optimal threshold.

The amplitude sums of each threshold are sorted, and the matrix of $\boldsymbol{S}_I$ after sorting is denoted as $\tilde{\boldsymbol{S}}_I$. For better estimation, the L_0 amplitude sums of each threshold are selected, and the sequence of $\{\tilde{\boldsymbol{S}}_I(w, \tilde{l})\}_{1\times L_0}, \tilde{l} = 1, 2, \cdots, L_0$ is generated. Afterward, the variance of $\{\tilde{\boldsymbol{S}}_I(w, \tilde{l})\}_{1\times L_0}$ is calculated as v_w, and the variance sequence of $\{v_w\}_{1\times W}$ can be formed. The width of ship body can be estimated as follows:

$$D_{\text{s}} = 2D_{\text{opt}} = 2d_{w_{\text{opt}}} \tag{12}$$

$$w_{\text{opt}} = \arg\max_{w} \{v_w\}_{1\times W} \tag{13}$$

where

$$v_w = \frac{1}{L_0 - 1} \times \sum_{\tilde{l}} \left| \tilde{s}_I\left(k_{w\tilde{l}}, b_{w\tilde{l}}; d_w\right) - \frac{1}{L_0}\sum_{\tilde{l}} \tilde{s}_I\left(k_{w\tilde{l}}, b_{w\tilde{l}}; d_w\right) \right|^2. \tag{14}$$

The extracting precision of ship centerline can be improved greatly with the optimal distance threshold. For improving the robust performance, a novel cost function is proposed to overcome the influence of randomness, ship superstructure, and low SNR.

Since the energy of noise covered by the line group is lower than that of ship target, the proposed cost function can be defined as the amplitude sum. Then, the optimal line parameters can be obtained as follows:

$$(k_{\text{opt}}, b_{opt}) = \arg\max_{k,b} \mathbf{s}_I\left(D_{\text{opt}}\right) \tag{15}$$

where $\boldsymbol{s}_I(D_{\text{opt}}) = \{s_I(k_{w_{\text{opt}}l}, b_{w_{\text{opt}}l}; D_{\text{opt}})\}_{1\times L}$.

The flowchart of the proposed approach is demonstrated in Fig. 6, and the main procedures are as follows.

Step 1: Initialize the parameters.
The iteration number is set as L, the scope of threshold is set as $\{d_1, d_2, \cdots, d_W\}$, $d_1 = 0$, and $d_W = \min\{M, N\}/2$. Here, $N = \max\{y_t\} - \min\{y_t\}$, and $M = \max\{x_t\} - \min\{x_t\}$.
Step 2: Implement the conventional RANSAC algorithm, calculate the matrix of amplitude sum via (8) and (9), and obtain the matrices of slope and intercept in (10) and (11).
Step 3: Sort the matrix of $\boldsymbol{S}_I$, and obtain the matrix of $\tilde{\boldsymbol{S}}_I$.
Step 4: Select the L_0 maximums in each row of $\tilde{\boldsymbol{S}}_I$, and generate the W sequences of $\{\tilde{\boldsymbol{S}}_I(w, \tilde{l})\}_{1\times L_0}$.
Here, L_0 can be selected as $L/2$ because the energy of ship body is larger than the half-energy of entire ship target.
Step 5: Calculate variance of $\{\tilde{\boldsymbol{S}}_I(w, \tilde{l})\}_{1\times L_0}$, and generate variance sequence of $\{v_w\}_{1\times W}$.
Step 6: Estimate the width of ship body with (12) and (13), and obtain the optimal distance threshold of D_{opt}.
Step 7: Estimate the optimal line parameters of $(k_{\text{opt}}, b_{opt})$ via (15).

Here, the conventional RANSAC algorithm can be repeated for more than L times to improve the extracting precision.

The proposed approach can overcome the defect of randomness compared with the conventional RANSAC algorithm. The randomness of RANSAC algorithm is produced mainly by the operation of selecting initial samples randomly, whereas the proposed approach alleviates this issue via the estimation of ship body and the better cost function. The results of an

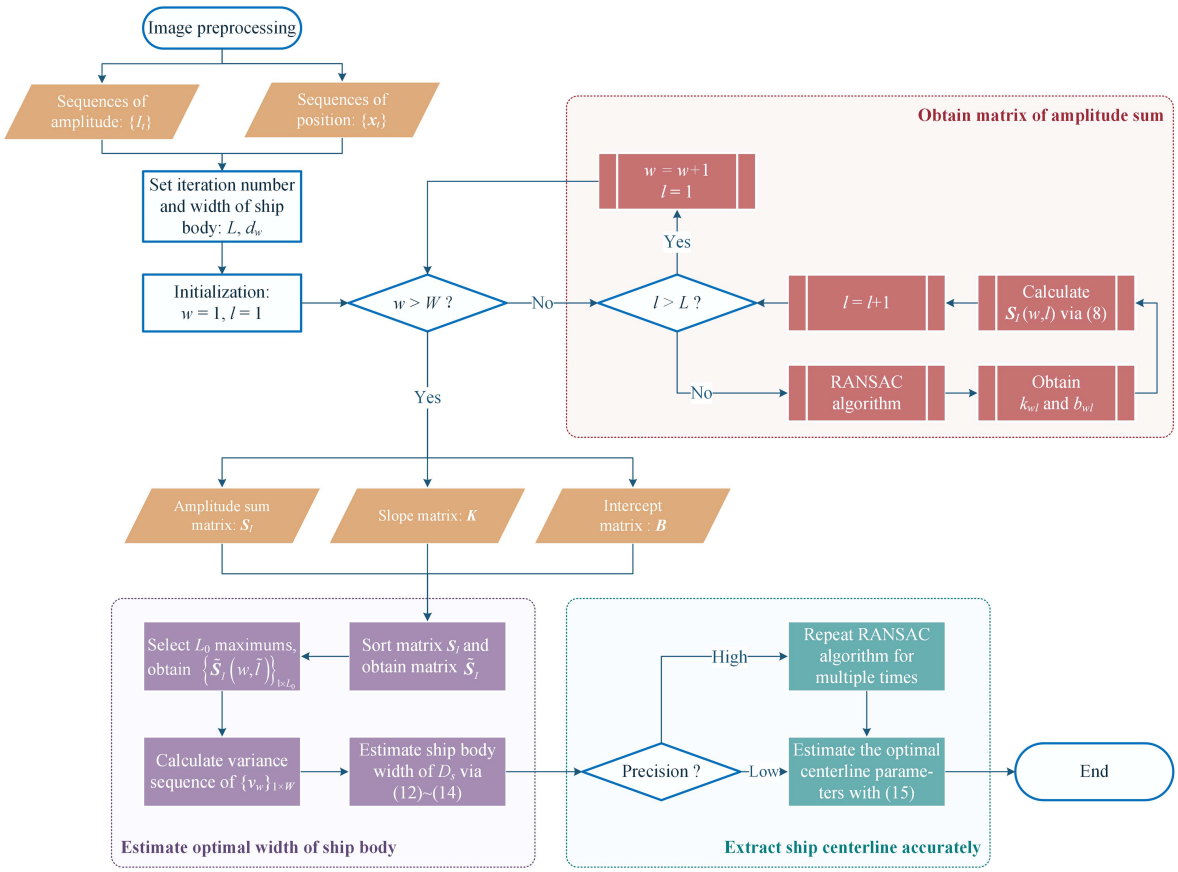

Fig. 6. Flowchart of novel approach for ship centerline extraction.

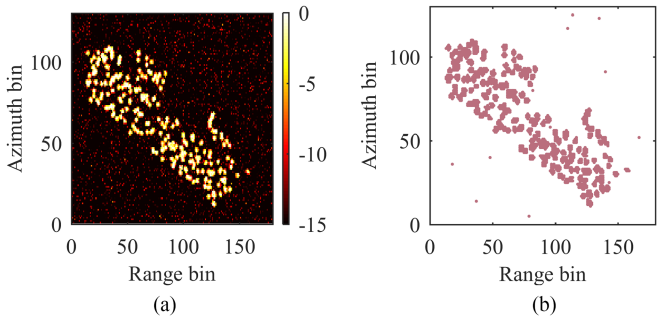

Fig. 7. Radar image and scatterer distribution. (a) Radar image. (b) Extraction result for scatterers.

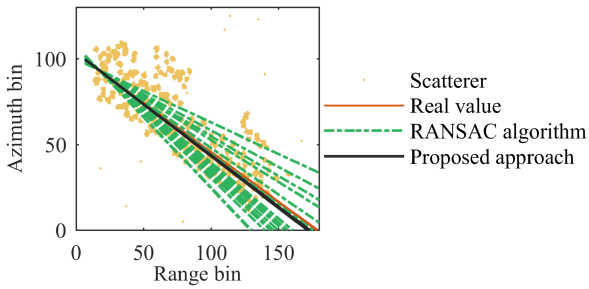

Fig. 8. Extraction results of ship centerline via the RANSAC algorithm and the proposed approach.

additional simulation are exhibited for illustration. The selected radar image is displayed in Fig. 7(a), and the scatterer distribution is extracted as shown in Fig. 7(b). Here, the real slope value is −0.5774. The conventional RANSAC algorithm and the proposed approach are implemented to extract the centerline of ship target. The extraction procedure is repeated by multiple times, which are 15 times here, and the extraction results are summarized in Fig. 8. Apparently, the proposed approach is stable, while the conventional RANSAC algorithm presents the random extraction results. Furthermore, the absolute and relative errors of the estimated slope for the two methods are calculated, as given in Fig. 9(a) and (b), respectively, which depicts the randomness of RANSAC algorithm and the stability of the proposed approach.

V. Experimental Results for Novel Approach of Centerline Extraction With RANSAC Algorithm

The effectiveness and robustness of the proposed approach are verified in this section. Here, two scatterer models are employed. The first kind is the ship target with superstructure, and the height of superstructure will be changed to verify the robustness of the proposed approach. The second kind is the ship target without superstructure, and the noise energy will be increased to test the performance of the proposed approach under the low SNR.

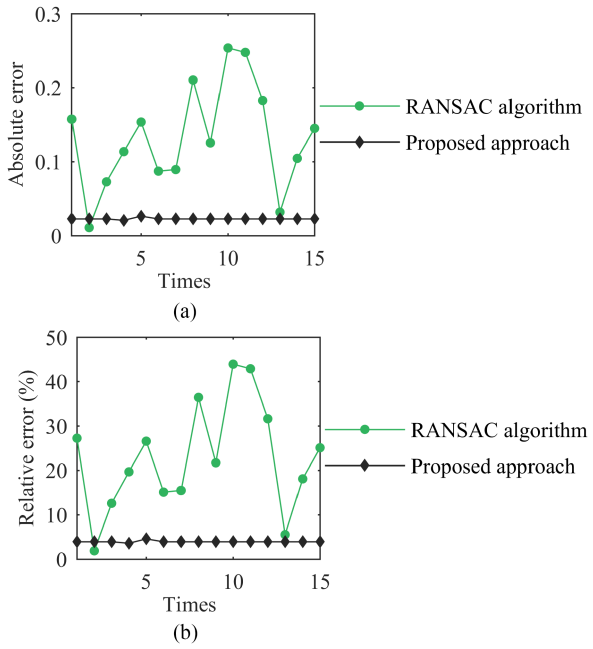

Fig. 9. Error comparisons of ship centerline for multiple times via the RANSAC algorithm and the proposed approach. (a) Comparison of absolute errors. (b) Comparison of relative errors.

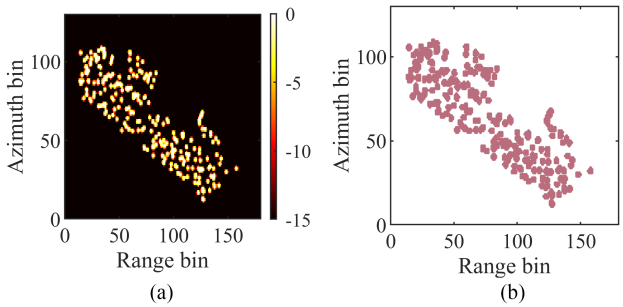

Fig. 10. Radar image and scatterer distribution. (a) Radar image. (b) Extraction result of scatterers.

Moreover, the LS method, Hough transform, and conventional RANSAC algorithm are utilized for comparing with the proposed approach.

A. Centerline Extraction Results of Simulated Data in the Case of Ship Superstructure

First, the radar image of ship target with superstructure is exhibited in Fig. 10(a), and the scatterers of ship target are extracted via the OTSU method, as given in Fig. 10(b).

Then, the sequences of image amplitude and position can be obtained. Within the range of distance threshold, the RANSAC algorithm is implemented repeatedly, and the matrix of amplitude sum can be calculated via (8) and (9), as shown in Fig. 11(a). When the width of ship body is small, the number of inliers and the sum of image amplitude are small. With enlarging the width of ship body, the number of inliers and the sum of image amplitude are increased and reach to the maximum. After sorting the matrix, the distribution of amplitude sum in Fig. 11(b) is attained, and the variance sequence is generated as demonstrated

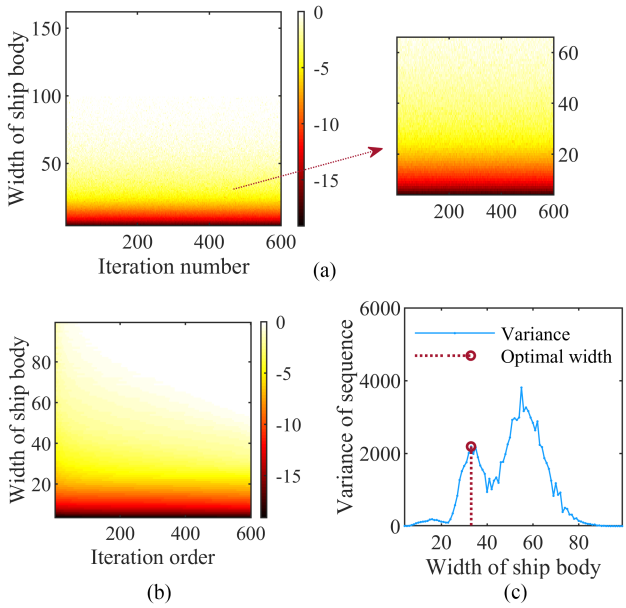

Fig. 11. Estimation results of ship body's width. (a) Distribution of amplitude sum before sorting. (b) Distribution of amplitude sum after sorting. (c) Variance of amplitude sum sequence.

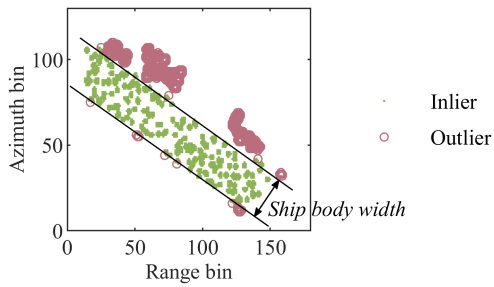

Fig. 12. Distribution of ship body with the proposed approach.

in Fig. 11(c). Obviously, two peak values exist in Fig. 11(c), which are located at 33 and 55, respectively. The optimal width of ship body is regarded as $D_s = 33$, and the width of entire ship target is considered as 55. The reason of two peaks is that the ship target has the apparent superstructure. Under this circumstance, the first peak position can be selected as the optimal width.

Hence, the distance threshold is determined as 16.5. The RANSAC algorithm is repeated for multiple times to improve the extraction precision. The distribution of ship body via the proposed approach is displayed in Fig. 12. Here, the green dot and the red circle show the inlier and outlier, respectively. Especially, the green inliers are distributed on the ship body, which illustrates that the width of ship body is estimated accurately.

Several conventional methods, including the LS method, Hough transform, and RANSAC algorithm, are applied for comparing with the extraction precision. The extraction results of ship centerline via different methods are contrasted in Fig. 13, in which the yellow dot is the scatterer of ship, the red, blue, green, and black lines represent the LS method, Hough transform, conventional RANSAC algorithm, and the proposed approach, respectively. Obviously, the proposed approach has the excellent extraction performance.

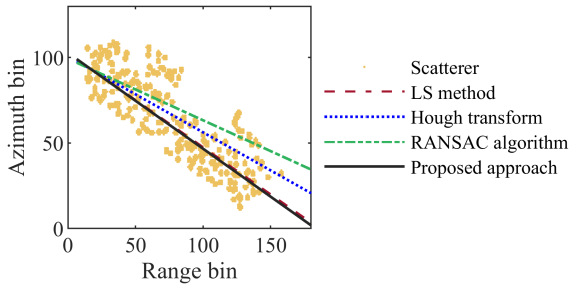

Fig. 13. Extraction results of ship centerline with different methods.

TABLE II
ESTIMATION RESULTS OF SHIP CENTERLINE WITH DIFFERENT METHODS

Category	LS method	Hough transform	RANSAC algorithm	Proposed approach
Estimated slope	−0.5515	−0.4452	−0.3603	−0.5606
Absolute error	0.0258	0.1321	0.2171	0.0167
Relative error (%)	4.4711	22.8841	37.5996	2.9002

TABLE III
ESTIMATION RESULTS OF SHIP CENTERLINE FOR THE SHIPS WITH DIFFERENT HEIGHTS OF SUPERSTRUCTURE

Multiple of super-structure height	LS method	Hough transform	RANSAC algorithm	Proposed approach
1.0	−0.5515	−0.4452	−0.7368	−0.5728
1.2	−0.5446	−1.0000	−0.5493	−0.5833
1.4	−0.5188	−1.0000	−0.6771	−0.5610
1.6	−0.5176	−1.0000	−0.6852	−0.5745
1.8	−0.3986	−0.4245	−0.3878	−0.5070
2.0	−0.4132	−0.6009	−0.5000	−0.5534

The estimated slopes of the ship centerline with different methods are summarized in Table II. The real value of slope is −0.5774. From the absolute and relative error, the proposed approach has the highest estimation precision.

Afterward, the robustness of the proposed method for the ship superstructure is measured. The height of superstructure in the scatterer model is increased gradually. For the ship target with the 1.0–2.0 multiple height of superstructure, the extraction results of ship centerline are demonstrated in Fig. 14(a)–(f), respectively. Obviously, the performance of LS method is degraded with the increased height, because the outliers generated by the superstructure are not eliminated. The estimation precision of Hough transform is poor as well due to the ship superstructure. The RANSAC algorithm performs unstably, which is induced by the randomness and inappropriate cost function. The proposed approach extracts the ship centerline most accurately, because it can eliminate the outliers and use the maximum amplitude sum as cost function.

The estimated slopes of ship centerline with different heights of superstructure are listed in Table III, and the real value of slope is −0.5774. The absolute and relative errors are given in Fig. 15(a) and (b), respectively. Apparently, the proposed method shows the higher precision. Hence, the proposed approach is robust for the ship target with superstructure.

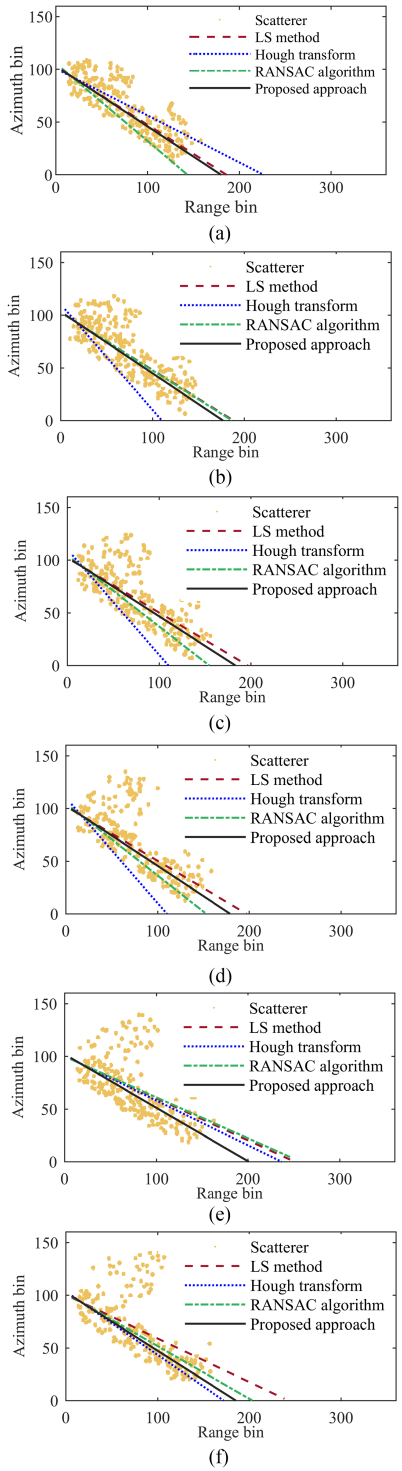

Fig. 14. Extraction results of ship centerline for the ships with different heights of superstructure. (a)–(f) Represent the cases of 1.0, 1.2, 1.4, 1.6, 1.8, and 2.0 times height of superstructure, respectively.

B. Centerline Extraction Results of Simulated Data in the Case of Low SNR

Here, the ship model without the superstructure is utilized for the low SNR environment. First, the SNR is set as 0 dB, and the radar image and the extracted samples are shown in

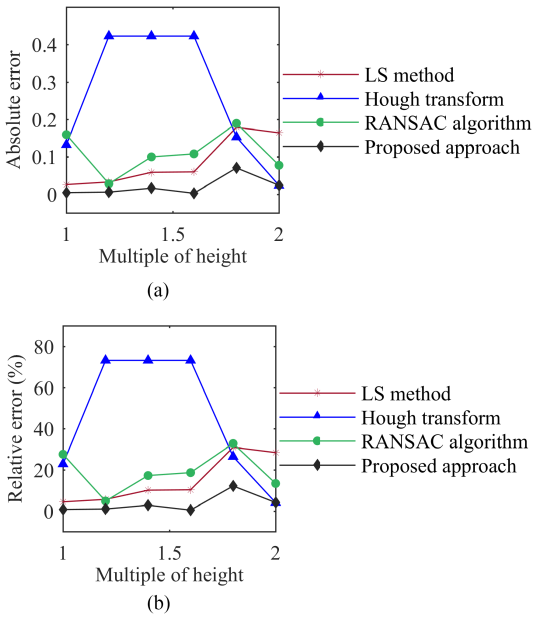

Fig. 15. Error comparisons of ship centerline for the ships with different heights of superstructure. (a) Comparison of absolute errors. (b) Comparison of relative errors.

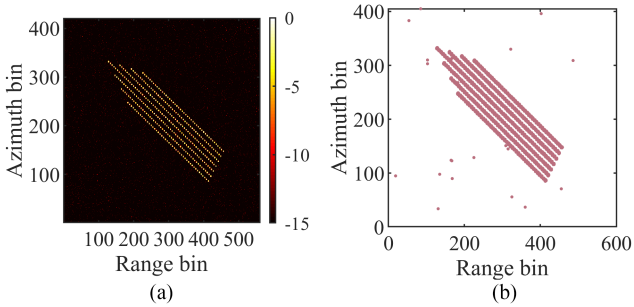

Fig. 16. Radar image and scatterer distribution. (a) Radar image. (b) Extraction result of scatterers.

Fig. 16(a) and (b), respectively. Obviously, there are several abnormal samples in Fig. 16(b).

Then, the distributions of amplitude sum before and after sorting are demonstrated in Fig. 17(a) and (b), respectively. The variance sequence is shown in Fig. 17(c), in which only one peak exists, and the optimal width of ship body is $D_{\mathrm{s}} = 99$.

Hence, the distance threshold is set as $D_{\max} = 49.5$. With the proposed approach, the ship body is extracted as shown in Fig. 18, and the abnormal samples are eliminated.

The ship centerlines extracted by different methods are given in Fig. 19. Obviously, the Hough transform and conventional RANSAC algorithm have poor performance, while the proposed approach can extract the centerline accurately.

The estimated slopes via different methods are summarized in Table IV, and the real value of slope is -0.7002. Apparently, the proposed approach has the highest precision, while the LS method has lower precision owing to the low SNR.

Moreover, the proposed approach is robust under the low SNR. Here, the Monte Carlo experiment is implemented, the

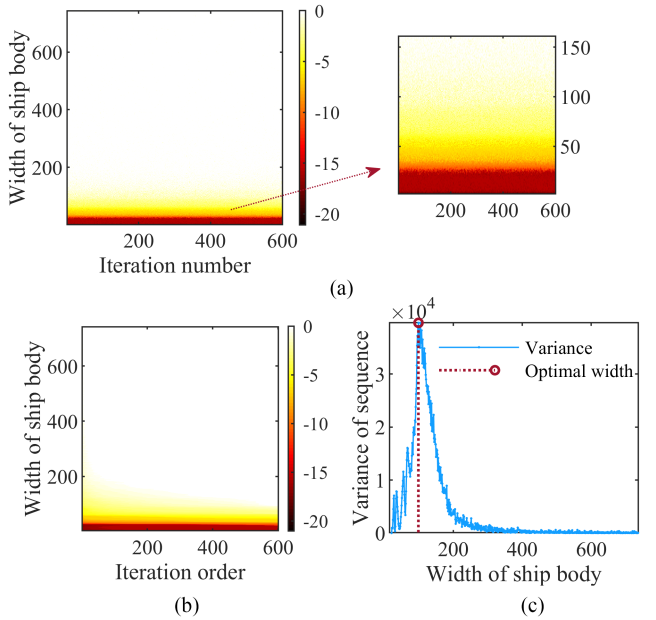

Fig. 17. Estimation results of ship body's width. (a) Distribution of amplitude sum before sorting. (b) Distribution of amplitude sum after sorting. (c) Variance of amplitude sum sequence.

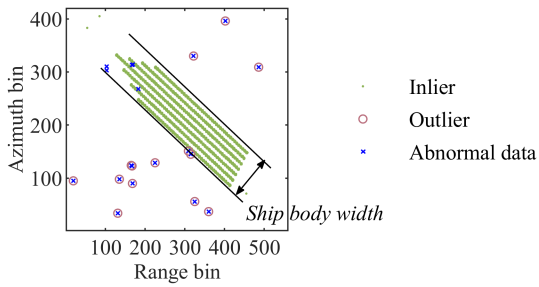

Fig. 18. Distribution of ship body with the proposed approach.

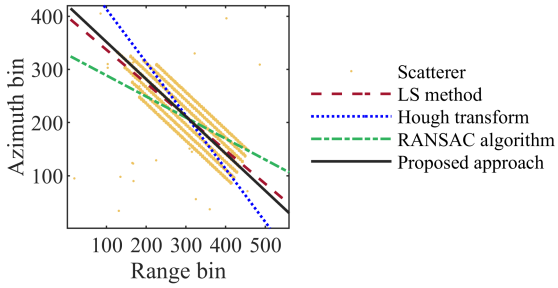

Fig. 19. Extraction results of ship centerline with different methods.

TABLE IV
ESTIMATION RESULTS OF SHIP CENTERLINE WITH DIFFERENT METHODS

Category	LS method	Hough transform	RANSAC algorithm	Proposed approach
Estimated slope	−0.6300	−1.0000	−0.3960	−0.7033
Absolute error	0.0702	0.2998	0.3042	0.0031
Relative error (%)	10.0298	42.8148	43.4397	0.4487

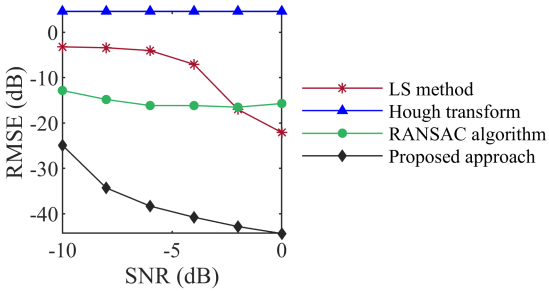

Fig. 20. Estimation error comparisons of ship centerline via Monte Carlo experiment under different SNRs.

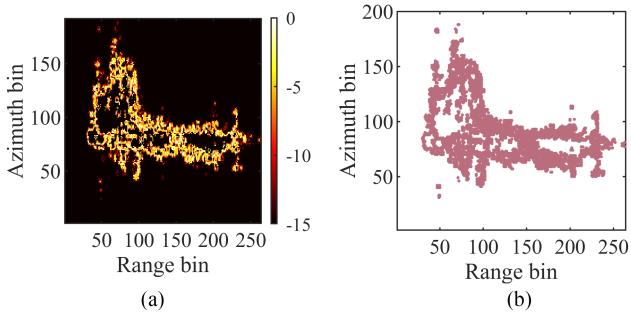

Fig. 21. Radar image and scatterer distribution. (a) Radar image. (b) Extraction result of scatterers.

SNRs are set as −10–0 dB, and each fitting method is repeated for 100 times, respectively.

The root mean square errors (RMSEs) produced by different methods are given in Fig. 20. Obviously, the Hough transform is stable under the low SNR, whereas its precision is relatively low. The performance of LS method is degraded with reducing the SNR. The conventional RANSAC algorithm shows better performance compared with the LS method, whereas its extraction precision is lower than the proposed approach.

C. Centerline Extraction Results of Real Measured Data

The radar images of the real measured data are used to extract the ship centerline. The shore-based ISAR works at X band, the pulse repetition frequency is 250 Hz, and the bandwidth is 400 MHz.

The radar image and scatterer distribution of the ship target are given in Fig. 21(a) and (b), respectively. Then, before and after sorting, the matrices of amplitude sum are displayed in Fig. 22(a) and (b), respectively. With calculating the variance sequence, the optimal width of ship body can be obtained as $D_s = 38$. With the optimal distance threshold, the ship body can be extracted, as observed in Fig. 23, where the inliers are distributed on the ship body. Meanwhile, we can see that the extraction result of the proposed approach is accurate and robust for the superstructure. The extraction results with different methods are contrasted in Fig. 24. Apparently, the performances of other methods are affected by the ship superstructure, and the proposed approach has the highest precision.

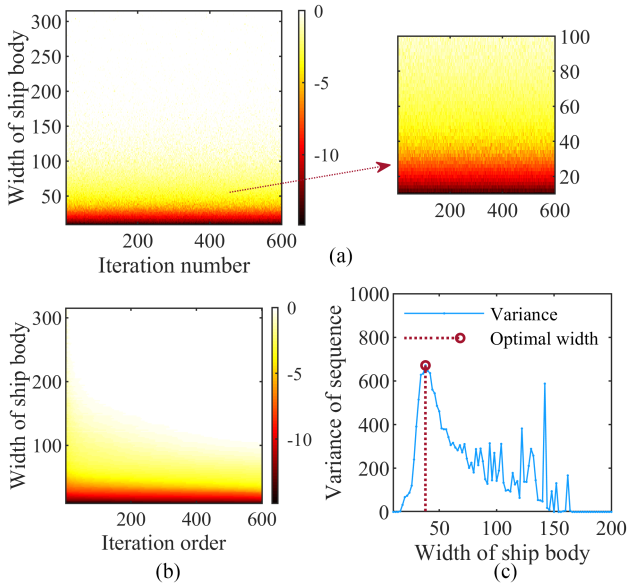

Fig. 22. Estimation results of ship body's width. (a) Distribution of amplitude sum before sorting. (b) Distribution of amplitude sum after sorting. (c) Variance of amplitude sum sequence.

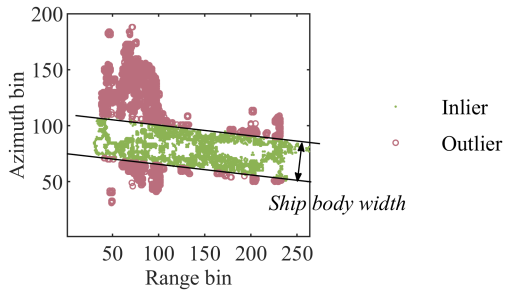

Fig. 23. Distribution of ship body with the proposed approach.

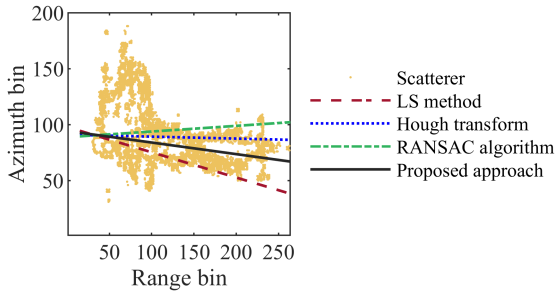

Fig. 24. Extraction results of ship centerline with different methods.

D. Analysis of Ship Centerline Extraction Results

The results in Section V-A–C illustrate that the performance of the proposed approach is superior to the other three methods. The reason of superiority is that the proposed approach can overcome the defects existing in these methods and improve the extraction precision and robustness consequently.

In the LS method, all the observation data are used for fitting straight line, which implies that some abnormal data deriving from the low SNR environment and ship superstructure cannot

be rejected. Hence, the performance of LS method is poorer when it applies in the domain of ship radar imaging.

The Hough transform is stable in the low SNR environment. As similar with the LS method, all the observation data are involved in the Hough integration for extracting straight line, therefore the precision of Hough transform is affected significantly by the ship superstructure. Moreover, the issue of multiple solution exists in the Hough transform, which is disadvantageous for the ship centerline extraction.

Different with the LS method and Hough transform, the conventional RANSAC algorithm can reject the abnormal data induced by the noise and ship superstructure. However, its performance is influenced strongly by the selection of initial samples and distance threshold. Furthermore, its cost function of maximal inliers number is inappropriate for the ship centerline extraction, which does not utilize the amplitude information of radar image adequately.

The proposed approach can overcome the defects of the aforementioned methods, which is characterized by the stability and has good robustness for the situation of low SNR and ship superstructure. First, the proposed approach utilizes the advantage of conventional RANSAC that the outliers arising from the low SNR and ship superstructure can be eliminated. Predictably, it has better performance in solving the issue of ship centerline extraction compared with LS method and Hough transform.

Second, the selection of distance threshold cannot degrade the extraction precision of the proposed approach compared with the conventional RANSAC algorithm, because it is well determined via the estimation of ship body width.

Third, a novel cost function of amplitude sum is applied in the proposed approach, which overcomes the randomness of the conventional RANSAC algorithm and further improves the extraction precision.

Hence, the proposed approach shows the better performance in the application of ship centerline extraction compared with the other methods.

VI. Experimental Results for Optimal Time Selection via the Proposed Approach

The proposed approach can be applied well in the field of optimal time selection. In this section, four different methods are implemented to represent the curve of centerline slope, which are LS method, Hough transform, conventional RANSAC algorithm, and the proposed approach. First, the ship centerlines in each time interval are extracted, which can reflect the vertical rotational motion of ship target. Then, the optimal time intervals are selected according to the theory in [22].

Predictably, the extracted ship centerlines are different via the various methods, which are related to the extraction precision. Hence, the different optimal time intervals will be selected. Some cases may appear, such that in the selected optimal time interval, the view of radar image should be a top or side view with the theoretical analysis, while the radar image shows the inverse (side or top) view or hybrid view actually. These cases can illustrate that the low extraction precision affects the optimal time interval selection.

In this section, the extraction results and the ship views in the ISAR images will be provided to reflect the performance of different extraction methods.

TABLE V
Parameters of Simulated Data

Category	Parameter	Value
ISAR system	Bandwidth	300 MHz
	Sample frequency	600 MHz
	Carrier frequency	10 GHz
	Pulse repetition frequency	400 Hz
	Pulse width	8 μs
	Central range	20 km
Ship Target	Translational velocity	1.5 m/s
	Rotational amplitude (roll)	5.5°
	Rotational period (roll)	23.2 s
	Rotational amplitude (pitch)	1.2°
	Rotational period (pitch)	14.6 s
	Rotational amplitude (yaw)	6.5°
	Rotational period (yaw)	16.2 s

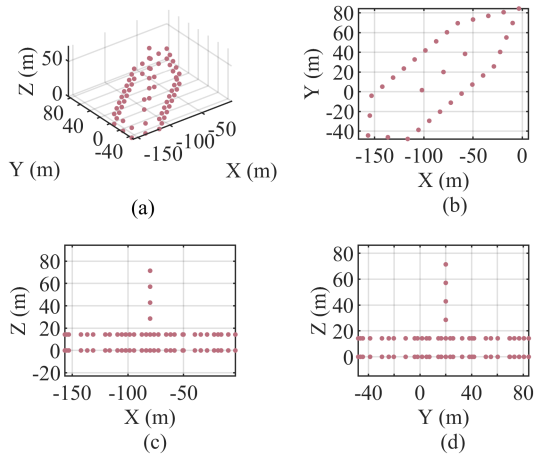

Fig. 25. Ship scatterer model. (a) 3-D view of scatterer model. (b) Top view of scatterer model. (c) Front view of scatterer model. (d) Side view of scatterer model.

A. Optimal Time Selection Results of Simulated Data

The parameters of ship target and ISAR system are summarized in Table V, and the ship target has the 3-D sinusoidal angular movement and translational movement. The 3-D view, top view, front view, and side view of ship scatterer model can be observed in Fig. 25(a)–(d), respectively. The SNR of echo is set as −5 dB to simulate the low SNR environment, and the ship target has the mast as the superstructure. The ship target is observed for up to 18.0 s, which is too long for ISAR imaging, and causes the azimuth defocus. Several ISAR images before selecting the optimal time interval are shown in Fig. 26, which are defocused and exhibit the ship's hybrid view. Therefore, the optimal time selection technique should be implemented.

First, the four extraction methods are adopted to generate the curves of centerline slope in Figs. 27(a)–30(a). The curves of

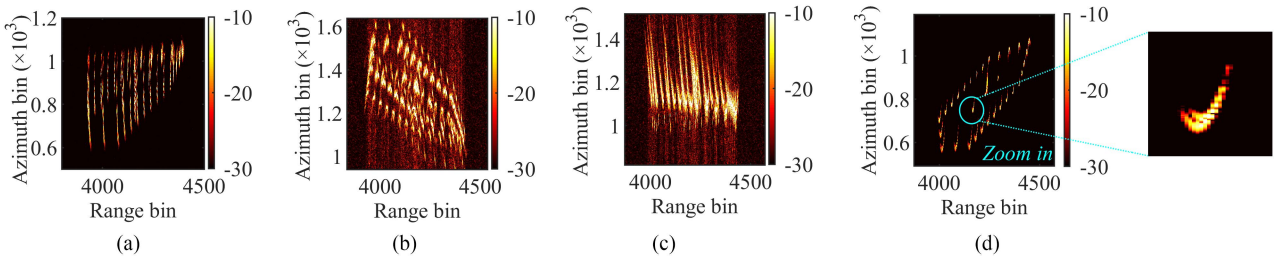

Fig. 26. Defocused ISAR images before optimal time selection. (a) Time interval of [0 s, 4.5 s]. (b) Time interval of [4.5 s, 9.0 s]. (c) Time interval of [9.0 s, 13.5 s]. (d) Time interval of [13.5 s, 18.0 s].

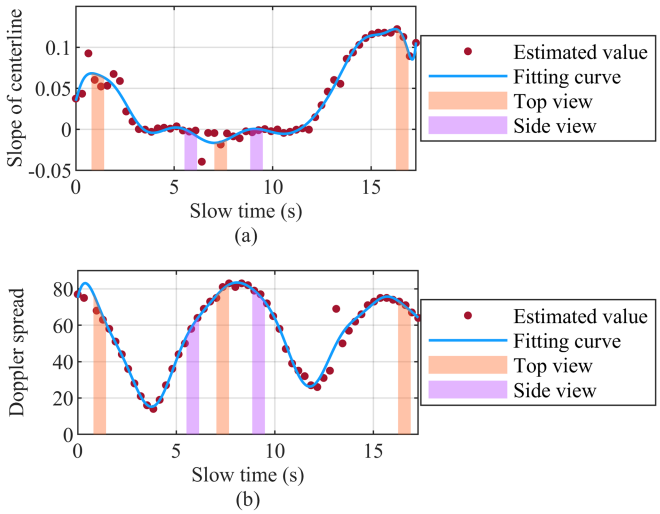

Fig. 27. Optimal time selection results via extracting ship centerline with LS method. (a) Curve of centerline slope with LS method. (b) Curve of Doppler spread.

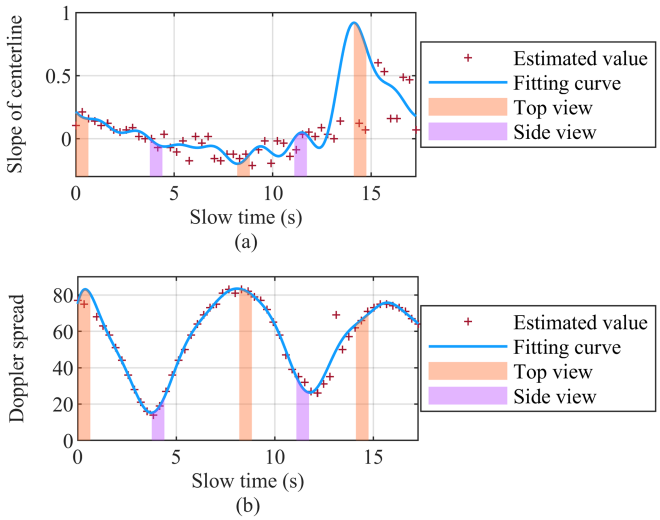

Fig. 28. Optimal time selection results via extracting ship centerline with Hough transform. (a) Curve of centerline slope with Hough transform. (b) Curve of Doppler spread.

Doppler spread are same in Figs. 27(b)–30(b), which reveal the obvious shape of sinusoidal curve. Here, the curve is produced by the Fourier fitting with the minimal RMSE, which is appropriate considering the sinusoidal rotation movement.

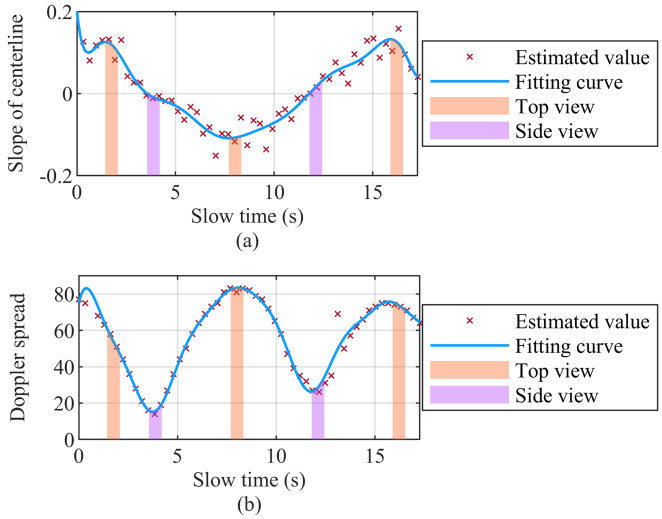

Fig. 29. Optimal time selection results via extracting ship centerline with conventional RANSAC algorithm. (a) Curve of centerline slope with conventional RANSAC algorithm. (b) Curve of Doppler spread.

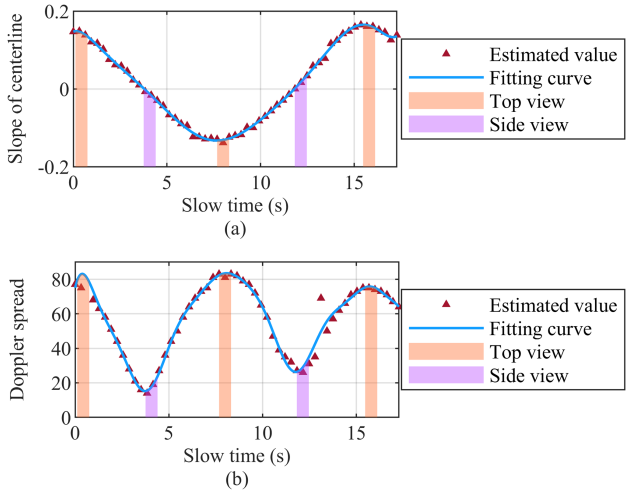

Fig. 30. Optimal time selection results via extracting ship centerline with the proposed approach. (a) Curve of centerline slope with the proposed approach. (b) Curve of Doppler spread.

The curves in Figs. 27(a) and 28(a) are deficient in the shape of sine owing to the poor extraction precision of LS method and Hough transform. The curves in Figs. 29(a) and 30(a) demonstrate the expectative sinusoidal shape, which reflect the higher precision of RANSAC algorithm and proposed

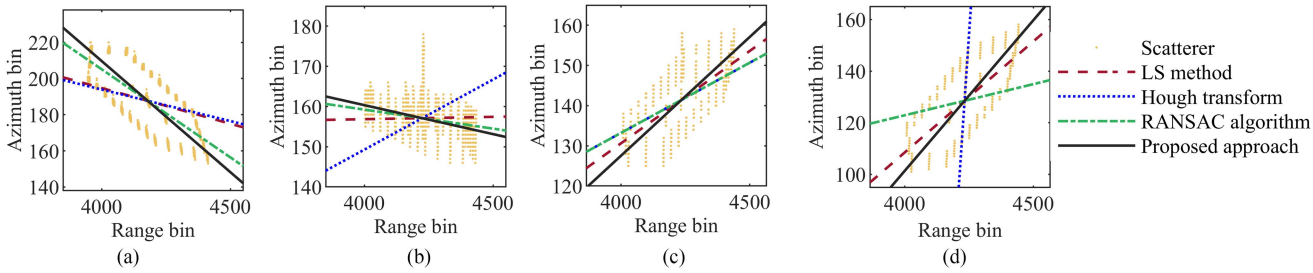

Fig. 31. Examples of extraction result via different ship centerline extraction methods. (a) Example 1. (b) Example 2. (c) Example 3. (d) Example 4.

TABLE VI
OPTIMAL IMAGING TIME INTERVALS VIA DIFFERENT SHIP CENTERLINE EXTRACTION METHODS FOR SIMULATED DATA

Time interval order / method	1	2	3	4	5
LS method	[0.80 s, 1.44 s]	[5.52 s, 6.16 s]	[7.04 s, 7.68 s]	[8.86 s, 9.50 s]	[16.26 s, 16.90 s]
Hough transform	[0.00 s, 0.64 s]	[3.76 s, 4.40 s]	[8.20 s, 8.84 s]	[11.10 s, 11.74 s]	[14.12 s, 14.76 s]
RANSAC algorithm	[1.44 s, 2.08 s]	[3.56 s, 4.20 s]	[7.70 s, 8.34 s]	[11.80 s, 12.44 s]	[15.90 s, 16.54 s]
Proposed approach	[0.11 s, 0.75 s]	[3.76 s, 4.40 s]	[7.68 s, 8.32 s]	[11.83 s, 12.47 s]	[15.48 s, 16.12 s]

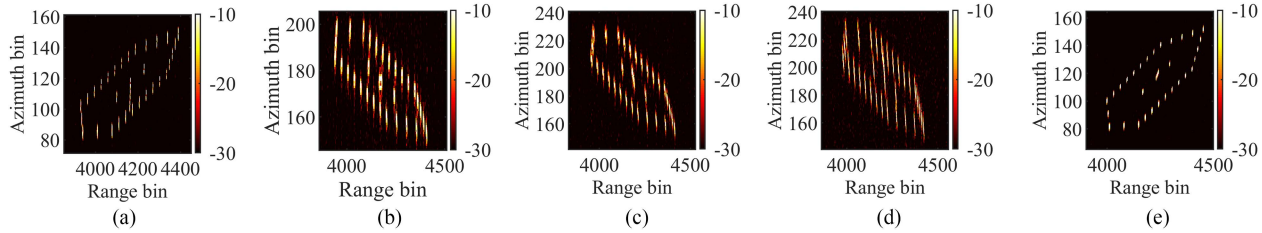

Fig. 32. ISAR imaging results of optimal time intervals via LS method. (a) Time interval of [0.80 s, 1.44 s]. (b) Time interval of [5.52 s, 6.16 s]. (c) Time interval of [7.04 s, 7.68 s]. (d) Time interval of [8.86 s, 9.50 s]. (e) Time interval of [16.26 s, 16.90 s].

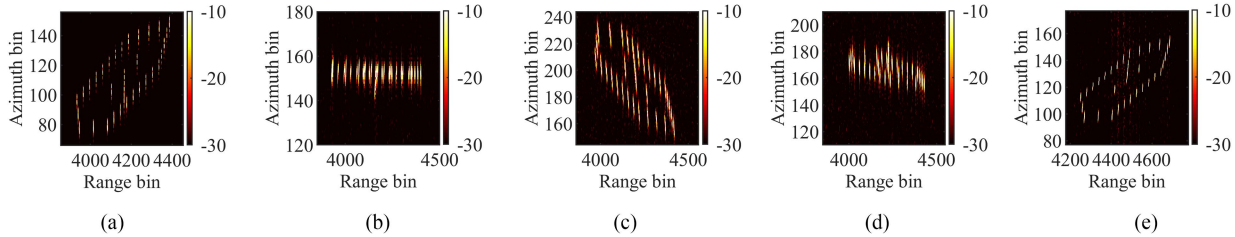

Fig. 33. ISAR imaging results of optimal time intervals via Hough transform. (a) Time interval of [0.00 s, 0.64 s]. (b) Time interval of [3.76 s, 4.40 s]. (c) Time interval of [8.20 s, 8.84 s]. (d) Time interval of [11.10 s, 11.74 s]. (e) Time interval of [14.12 s, 14.76 s].

approach. Whereas, the disturbance can be observed apparently in Fig. 29(a), which is induced by the inappropriate cost function and randomness of RANSAC algorithm. Moreover, the distance threshold of RANSAC algorithm is set by estimating the ship body width, without which the curve shape will be not closed to the sinusoidal shape.

Several examples of extraction results with different methods are contrasted in Fig. 31(a)–(d). Obviously, the proposed approach can extract the ship centerline more accurately, while other methods produce larger errors due to the low SNR environment and ship superstructure. As given earlier, the proposed approach characterizes better performance.

With the theory in [22], the optimal time intervals are exported, as described in the orange and purple area in Figs. 27–30. These optimal time intervals are summarized in Table VI. Theoretically, the radar images yielded by the time intervals in Table VI should feature as single view of ship, whereas the unexpected hybrid-view results may appear owing to the extraction errors. The ISAR imaging results corresponding to the time intervals in Table VI are exhibited in Figs. 32–35. Apparently, some of these results represent the unexpected hybrid view, such as in Figs. 33(d), 34(b), and (e). Moreover, Table VII lists the theoretical views of ship corresponding to the time intervals in Table VI, and gives the actual views of ship

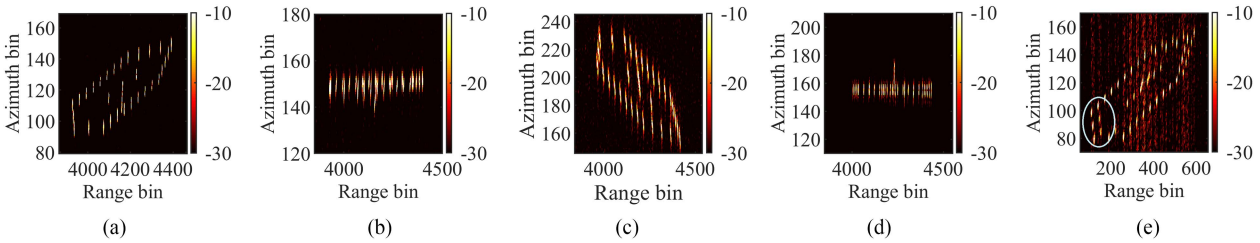

Fig. 34. ISAR imaging results of optimal time intervals via conventional RANSAC algorithm. (a) Time interval of [1.44 s, 2.08 s]. (b) Time interval of [3.56 s, 4.20 s]. (c) Time interval of [7.70 s, 8.34 s]. (d) Time interval of [11.80 s, 12.44 s]. (e) Time interval of [15.90 s, 16.54 s].

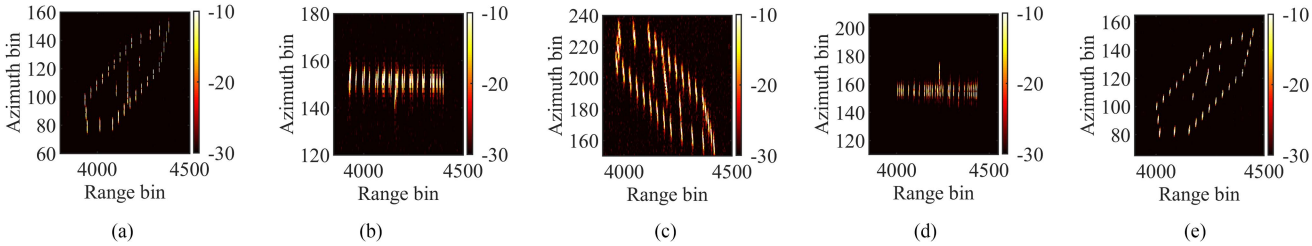

Fig. 35. ISAR imaging results of optimal time intervals via the proposed approach. (a) Time interval of [0.11 s, 0.75 s]. (b) Time interval of [3.76 s, 4.40 s]. (c) Time interval of [7.68 s, 8.32 s]. (d) Time interval of [11.83 s, 12.47 s]. (e) Time interval of [15.48 s, 16.12 s].

TABLE VII
COMPARISON OF SHIP VIEWS IN DIFFERENT OPTIMAL IMAGING TIME INTERVALS FOR SIMULATED DATA

method \ Time interval order		1	2	3	4	5
LS method	Theorization	Top view	Side view	Top view	Side view	Top view
	Reality	Top view	***Top view***	Top view	***Top view***	Top view
Hough transform	Theorization	Top view	Side view	Top view	Side view	Top view
	Reality	Top view	Side view	Top view	***Hybrid view***	Top view
RANSAC algorithm	Theorization	Top view	Side view	Top view	Side view	Top view
	Reality	Top view	***Hybrid view***	Top view	Side view	***Hybrid view***
Proposed approach	Theorization	Top view	Side view	Top view	Side view	Top view
	Reality	Top view	Side view	Top view	Side view	Top view

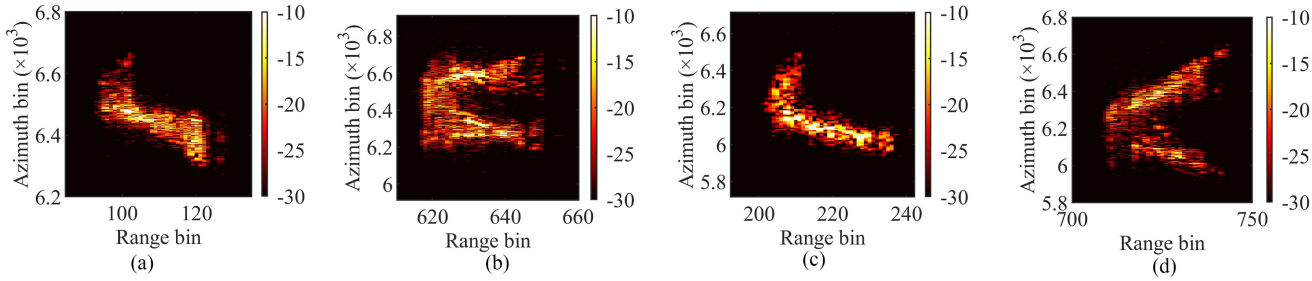

Fig. 36. Defocused ISAR images before optimal time selection. (a) Time interval of [0 s, 13.8240]. (b) Time interval of [13.8240 s, 27.6480 s]. (c) Time interval of [27.6480 s, 41.4720 s]. (d) Time interval of [41.4780 s, 55.2960 s].

in Figs. 32–35. Obviously, the unsatisfying circumstance that the actual view does not match the theoretical view appears in the results of LS method, Hough transform, and conventional RANSAC algorithm, which is induced by the poor extraction results of ship centerline.

Hence, the extraction of ship centerline with high accuracy is significant for the optimal time selection. Compared with other methods, we can see that the proposed approach shows higher precision, and has wide applicability in the field of radar imaging.

Remark 1: The selection of optimal time interval is related to the estimation of vertical rotational motion, which can be reflected by the slope of ship centerline. Hence, when the ship centerline cannot be extracted accurately, the selected optimal time interval will be incorrect. For the other methods (LS, Hough transform, and RANSAC algorithm), their extraction precisions

TABLE VIII
PARAMETERS OF REAL MEASURED DATA

Category	Parameter	Value
ISAR system	Bandwidth	200 MHz
	Pulse repetition frequency	500 Hz
	Carrier frequency	X band
	Entire imaging interval	55.296 s
	Number of range bin	962

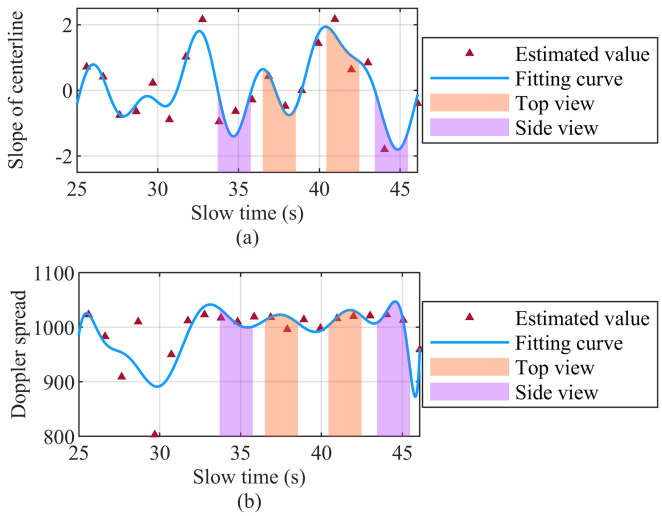

Fig. 37. Optimal time selection results via extracting ship centerline with LS method. (a) Curve of centerline slope with LS method. (b) Curve of Doppler spread.

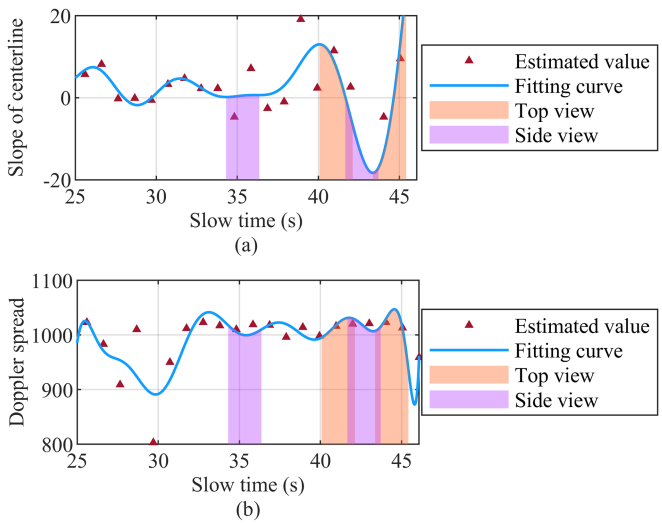

Fig. 38. Optimal time selection results via extracting ship centerline with Hough transform. (a) Curve of centerline slope with Hough transform. (b) Curve of Doppler spread.

of ship centerline are lower, therefore the actual result may not match the theoretical analysis. Some cases may appear, such that in the selected optimal time interval, the view of radar image should be a top or side view with the theoretical analysis, while the radar image shows the inverse (side or top) view or hybrid view actually.

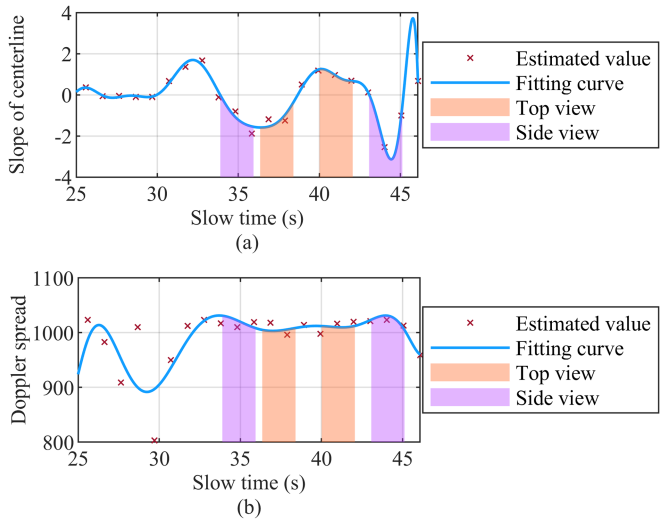

Fig. 39. Optimal time selection results via extracting ship centerline with conventional RANSAC algorithm. (a) Curve of centerline slope with conventional RANSAC algorithm. (b) Curve of Doppler spread.

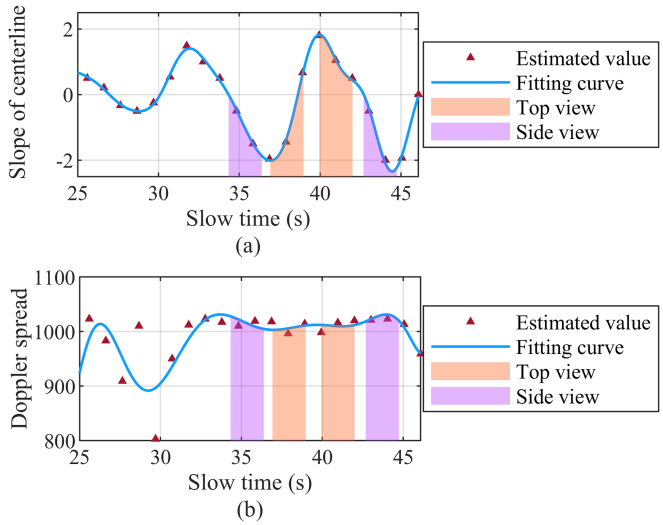

Fig. 40. Optimal time selection results via extracting ship centerline with the proposed approach. (a) Curve of centerline slope with the proposed approach. (b) Curve of Doppler spread.

B. Optimal Time Selection Results of Real Measured Data

The parameters of real measured data are summarized in Table VIII, and the extra 0 dB-noise is added. The entire imaging interval is long, and the ISAR images without the optimal time selection are listed in Fig. 36, which are defocused and show the hybrid views. For obtaining the focused and single-view ISAR image, part of the entire imaging interval is used for optimal time selection.

The four extraction methods of ship centerline are applied, and the curves of centerline slope are shown in Figs. 37(a)–40(a). Clearly, these curves are distinct, and the curve via the proposed approach depicts the best shape of sine. The curves of Doppler spread are same in Figs. 37(b)–40(b). Based on the theory in [22], the optimal time intervals are selected, as labeled in the orange and purple area in Figs. 37–40.

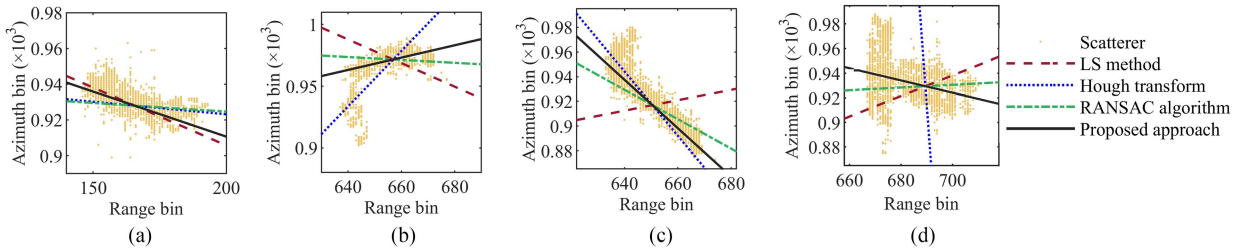

Fig. 41. Examples of extraction result via different ship centerline extraction methods. (a) Example 1. (b) Example 2. (c) Example 3. (d) Example 4.

TABLE IX
OPTIMAL IMAGING TIME INTERVALS VIA DIFFERENT SHIP CENTERLINE EXTRACTION METHODS FOR REAL MEASURED DATA

Time interval order / method	1	2	3	4
LS method	[33.7100s, 35.7580s]	[36.5000s, 38.5480s]	[40.4300s, 42.4780s]	[43.4300s, 45.4780s]
Hough transform	[34.3100s, 36.3580s]	[40.0700s, 42.1180s]	[41.6600s, 43.7080s]	[43.3700s, 45.4180s]
RANSAC algorithm	[33.8900s, 35.9380s]	[36.3500s, 38.3980s]	[40.0100s, 42.0580s]	[43.0700s, 45.1180s]
Proposed approach	[34.3400s, 36.3880s]	[36.9200s, 38.9680s]	[39.9500s, 41.9980s]	[42.6800s, 44.7280s]

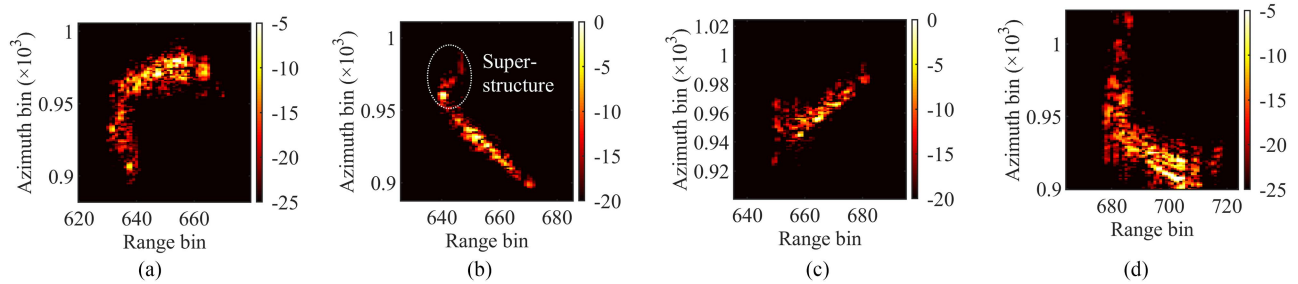

Fig. 42. ISAR imaging results of optimal time intervals via LS method. (a) Time interval of [33.7100 s, 35.7580 s]. (b) Time interval of [36.5000 s, 38.5480 s]. (c) Time interval of [40.4300 s, 42.4780 s]. (d) Time interval of [43.4300 s, 45.4780 s].

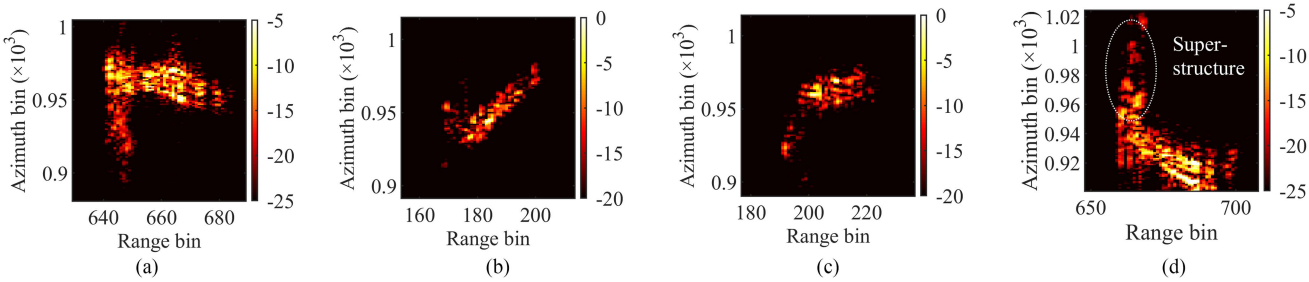

Fig. 43. ISAR imaging results of optimal time intervals via Hough transform. (a) Time interval of [34.3100 s, 36.3580 s]. (b) Time interval of [40.0700 s, 42.1180 s]. (c) Time interval of [41.6600 s, 43.7080 s]. (d) Time interval of [43.3700 s, 45.4180 s].

Several examples are demonstrated in Fig. 41 for comparing the extraction results of the four methods. Visibly, the proposed approach extracts the ship centerline accurately.

The selected time intervals are summarized in Table IX, with which the ISAR imaging results are exhibited in Figs. 42–45. Obviously, some hybrid views exist in Figs. 42(b), 43(d), 44(b) and (c), which show the unexpected ship superstructure. The actual and theoretical views of ship in Figs. 42–45 are summarized in Table X. Apparently, the actual results conform to the theoretical analysis in the proposed approach, whereas several unmatched results appear in other methods.

As given earlier, the proposed approach has superior performance and is suitable for the optimal time selection.

Remark 2: Recently, the deep learning technique is popular and applied extensively in the domain of image processing. Some methods for detecting straight line with the deep learning technique are proposed, such as line convolutional neural network, improved line segment detection, *etc*. In this kind of methods, the data set should be obtained as prior information, then the line feature is extracted assisted with the traditional detection straight line method generally, finally these line features are analyzed by the learning pool to detect the straight line.

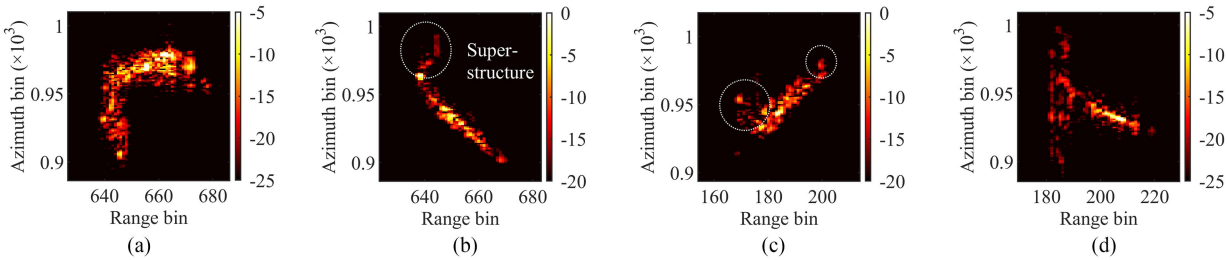

Fig. 44. ISAR imaging results of optimal time intervals via conventional RANSAC algorithm. (a) Time interval of [33.8900 s, 35.9380 s]. (b) Time interval of [36.3500 s, 38.3980 s]. (c) Time interval of [40.0100 s, 42.0580 s]. (d) Time interval of [43.0700 s, 45.1180 s].

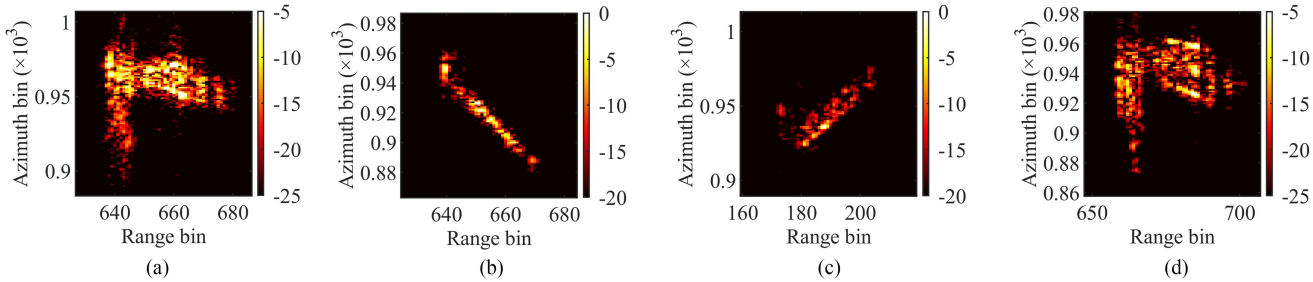

Fig. 45. ISAR imaging results of optimal time intervals via the proposed approach. (a) Time interval of [34.3400 s, 36.3880 s]. (b) Time interval of [36.9200 s, 38.9680 s]. (c) Time interval of [39.9500 s, 41.9980 s]. (d) Time interval of [42.6800 s, 44.7280 s].

TABLE X
COMPARISON OF SHIP VIEWS IN DIFFERENT OPTIMAL IMAGING TIME INTERVALS FOR REAL MEASURED DATA

method \ Time interval order		1	2	3	4
LS method	Theorization	Side view	Top view	Top view	Side view
	Reality	Side view	***Hybrid view***	Top view	Side view
Hough transform	Theorization	Side view	Top view	Side view	Top view
	Reality	Side view	Top view	***Hybrid view***	***Side view***
RANSAC algorithm	Theorization	Side view	Top view	Top view	Side view
	Reality	Side view	***Hybrid view***	***Hybrid view***	***Hybrid view***
Proposed approach	Theorization	Side view	Top view	Top view	Side view
	Reality	Side view	Top view	Top view	Side view

With the deep learning technique, the detecting robustness and precision can be improved under some complicated cases, such as low SNR condition.

VII. CONCLUSION

The ship centerline extraction is the key procedure for the optimal time selection. The ship superstructure and low SNR influence the extraction precision of ship centerline and the obtainment of single-view ISAR image consequently. To address this issue, a novel approach of ship centerline extraction with the RANSAC algorithm is proposed in this article. First, the width of ship body is estimated to determine the optimal distance threshold, which can improve the extraction precision. Second, a novel cost function of the amplitude sum of inliers is proposed for overcoming the randomness. The proposed approach is robust in the case of ship superstructure and low SNR, which is illustrated adequately by the results of simulated and real measured data. Meanwhile, this article applies the proposed approach in the optimal time selection technique, and the results show the superior performance of the proposed approach.

REFERENCES

[1] P. Huang, X.-G. Xia, M. Zhan, X. Liu, G. Liao, and X. Jiang, "ISAR imaging of a maneuvering target based on parameter estimation of multicomponent cubic phase signals," *IEEE Trans. Geosci. Remote Sens.*, vol. 60, Jan. 2022, Art. no. 5103918.

[2] M. Martorella, D. Pastina, F. Berizzi, and P. Lombardo, "Spaceborne radar imaging of maritime moving targets with the Cosmo-SkyMed SAR system," *IEEE J. Sel. Topics Appl. Earth Observ. Remote Sens.*, vol. 7, no. 7, pp. 2797–2810, Jul. 2014.

[3] Z.-Z. Huang et al., "Azimuth location deambiguity for SAR ground moving targets via coprime adjacent arrays," *IEEE J. Sel. Topics Appl. Earth Observ. Remote Sens.*, vol. 11, no. 2, pp. 551–561, Feb. 2018.

[4] S. Shao, H. Liu, L. Zhang, P. Wang, and J. Wei, "Integration of super-resolution ISAR imaging and fine motion compensation for complex maneuvering ship targets under high sea state," *IEEE Trans. Geosci. Remote Sens.*, vol. 60, Mar. 2022, Art. no. 5222820.

[5] S. Zhao, Z. Zhang, W. Guo, and Y. Luo, "An automatic ship detection method adapting to different satellites SAR images with feature alignment and compensation loss," *IEEE Trans. Geosci. Remote Sens.*, vol. 60, Apr. 2022, Art. no. 5225217.

[6] Y. Qian and D. Zhu, "High-resolution SAR imaging from azimuth periodically gapped raw data via generalised orthogonal matching pursuit," *Electron. Lett.*, vol. 54, pp. 1235–1237, Oct. 2018.
[7] G. Li, H. Zhang, X. Wang, and X.-G. Xia, "ISAR 2-D imaging of uniformly rotating targets via matching pursuit," *IEEE Trans. Aerosp. Electron. Syst.*, vol. 48, no. 2, pp. 1838–1846, Apr. 2012.
[8] Y. Yuan, Y. Luo, L. Kang, J. Ni, and Q. Zhang, "Range alignment in ISAR imaging based on deep recurrent neural network," *IEEE Geosci. Remote Sens. Lett.*, vol. 19, Mar. 2022, Art. no. 4022405.
[9] J. Zheng, H. Liu, G. Liao, T. Su, Z. Liu, and Q. H. Liu, "ISAR imaging of targets with complex motions based on a noise-resistant parameter estimation algorithm without nonuniform axis," *IEEE Sens. J.*, vol. 16, no. 8, pp. 2509–2518, Apr. 2016.
[10] G. Xu, M.-D. Xing, X.-G. Xia, Q.-Q. Chen, L. Zhang, and Z. Bao, "High-resolution inverse synthetic aperture radar imaging and scaling with sparse aperture," *IEEE J. Sel. Topics Appl. Earth Observ. Remote Sens.*, vol. 8, no. 8, pp. 4010–4027, Aug. 2015.
[11] X. Bai, F. Zhou, M. Xing, and Z. Bao, "High resolution ISAR imaging of targets with rotating parts," *IEEE Trans. Comput. Imag.*, vol. 47, no. 4, pp. 2530–2543, Oct. 2011.
[12] P. Zhou, M. Martorella, X. Zhang, Y. Dai, W. Sun, and Y. Wan, "Circular scan ISAR mode super-resolution imaging of ships based on a combination of data extrapolation and compressed sensing," *IEEE Sens. J.*, vol. 19, no. 16, pp. 6883–6894, Aug. 2019.
[13] P. Huang et al., "High-resolution ISAR imaging for maneuvering targets based on iterative adaptive processing," *IEEE Trans. Comput. Imag.*, vol. 7, pp. 1093–1108, Oct. 2021.
[14] L. Liu, F. Zhou, M. Tao, P. Sun, and Z. Zhang, "Adaptive translational motion compensation method for ISAR imaging under low SNR based on particle swarm optimization," *IEEE J. Sel. Topics Appl. Earth Observ. Remote Sens.*, vol. 8, no. 11, pp. 5146–5157, Nov. 2015.
[15] W. Rao, G. Li, X. Wang, and X.-G. Xia, "Adaptive sparse recovery by parametric weighted L_1 minimization for ISAR imaging of uniformly rotating targets," *IEEE J. Sel. Topics Appl. Earth Observ. Remote Sens.*, vol. 6, no. 2, pp. 942–952, Apr. 2013.
[16] X. Bai, X. Zhou, F. Zhang, L. Wang, R. Xue, and F. Zhou, "Robust Pol-ISAR target recognition based on ST-MC-DCNN," *IEEE Trans. Geosci. Remote Sens.*, vol. 57, no. 12, pp. 9912–9927, Dec. 2019.
[17] G. Xu, M.-D. Xing, L. Zhang, J. Duan, Q.-Q. Chen, and Z. Bao, "Sparse apertures ISAR imaging and scaling for maneuvering targets," *IEEE J. Sel. Topics Appl. Earth Observ. Remote Sens.*, vol. 7, no. 7, pp. 2942–2956, Jul. 2014.
[18] N. Li, Q. Shen, L. Wang, Q. Wang, Z. Guo, and J. Zhao, "Optimal time selection for ISAR imaging of ship targets based on time-frequency analysis of multiple scatterers," *IEEE Geosci. Remote Sens. Lett.*, vol. 19, Jan. 2022, Art. no. 4017505.
[19] R. Cao, Y. Wang, C. Yeh, Y. Zhang, and X. Lu, "A novel optimal time window determination approach for ISAR imaging of ship targets," *IEEE J. Sel. Topics Appl. Earth Observ. Remote Sens.*, vol. 15, pp. 3475–3503, May 2022.
[20] P. Zhou, X. Zhang, Y. Dai, W. Sun, and Y. Wan, "Time window selection algorithm for ISAR ship imaging based on instantaneous Doppler frequency estimations of multiple scatterers," *IEEE J. Sel. Topics Appl. Earth Observ. Remote Sens.*, vol. 12, no. 10, pp. 3799–3812, Oct. 2019.
[21] M. Martorella and F. Berizzi, "Time windowing for highly focused ISAR image reconstruction," *IEEE Trans. Aerosp. Electron. Syst.*, vol. 41, no. 3, pp. 992–1007, Jul. 2005.
[22] D. Pastina, A. Montanari, and A. Aprile, "Motion estimation and optimum time selection for ship ISAR imaging," in *Proc. IEEE Radar Conf.*, 2003, pp. 7–14.
[23] A. Noroozi and M. A. Sebt, "Weighted least squares target location estimation in multi-transmitter multi-receiver passive radar using bistatic range measurements," *IET Radar Sonar Navigation*, vol. 10, no. 6, pp. 1088–1097, Jul. 2016.
[24] A. H. Oveis and M. A. Sebt, "Coherent method for ground-moving target indication and velocity estimation using Hough transform," *IET Radar Sonar Navigation*, vol. 11, no. 4, pp. 646–655, Apr. 2017.
[25] J. Liu and F. Bu, "Improved RANSAC features image-matching method based on SURF," *J. Eng.*, vol. 2019, no. 23, pp. 9118–9122, Dec. 2019.
[26] P. Ploss, S. J. Rupitsch, and R. Lerch, "Extraction of spatial ultrasonic wave packet features by exploiting a modified hough transform," *IEEE Sens. J.*, vol. 14, no. 7, pp. 2389–2395, Jul. 2014.
[27] L.-L. Du, Y.-L. Xin, and Z.-P. Chen, "A new algorithm for ship centerline extraction in ISAR image," in *Proc. 2nd Int. Conf. Adv. Comput. Control*, 2010, pp. 213–216.
[28] N. Otsu, "A threshold selection method from gray-level histograms," *IEEE Trans. Syst., Man, Cybern.*, vol. 9, no. 1, pp. 62–66, Jan. 1979.

Rui Cao (Graduate Student Member, IEEE) was born in 1996. She received the B.S. degree in electronic information engineering from the Harbin Institute of Technology (HIT), Weihai, China, in 2018, and the M.S. degree in information and communication engineering in 2020 from HIT, Harbin, China, where she is currently working toward the Ph.D. degree in information and communication engineering.

Her current research interests include the field of radar imaging and radar signal processing.

Yong Wang (Senior Member, IEEE) was born in 1979. He received the B.S. and M.S. degrees in electronic engineering and the Ph.D. degree in information and communication engineering from the Harbin Institute of Technology (HIT), Harbin, China, in 2002, 2004, and 2008, respectively.

He is currently a Professor with the Institute of Electronic Engineering Technology, HIT. His main research interests are in the fields of time-frequency analysis of nonstationary signal, radar signal processing, and their application in synthetic aperture radar (SAR) imaging.

Dr. Wang has authored or coauthored more than 130 papers, most of them appeared in the journals of the IEEE TRANSACTIONS ON GEOSCIENCE AND REMOTE SENSING, *IET Signal Processing*, *Signal Processing*, etc. He received the Program for New Century Excellent Talents with the University of Ministry of Education of China in 2012, and the Excellent Doctor's Degree nomination Award in China in 2010.

Yun Zhang (Member, IEEE) was born in Heilongjiang, China, in November 1975. She received the B.S. and M.S. degrees in electronic engineering and the Ph.D. degree in information and communication engineering from the Harbin Institute of Technology (HIT), Harbin, China, in 2000, 2003, and 2009, respectively.

She is currently a Professor with the Research Institute of Electronic Engineering Technology, HIT. Her research interests include radar signal processing, SAR imaging, machine learning, and pattern analysis in remote sensing.

Mao Jian was born in Inner Monglia, China, in 1991. He received the B.S. degree in information science and electronic engineering from Zhejiang University, Hangzhou, Zhejiang, China, in 2014, and the M.S. degree from the Graduate School of the Second Academy of China Aerospace, Beijing, China, in 2017.

He is currently an Engineer with the Laboratory of Pinghu (Beijing Institute of Infinite Electric Measurement), Pinghu, China. His major research interests include radar signal and data processing.